TEL AVIV UNIVERSITY

The Iby and Aladar Fleischman Faculty of Engineering

The Zandman-Slaner School of Graduate Studies

Efficacy optimization of low frequency gas bubble-mediated sonoporation as a drug delivery platform to cancer cells

A thesis submitted toward the degree of

Master of Science in Biomedical Engineering

by

Michal Eck

This research was carried out in the Department of Biomedical Engineering

Under the supervision of Dr. Tali Ilovitsh

October 22

TEL AVIV UNIVERSITY

The Iby and Aladar Fleischman Faculty of Engineering

The Zandman-Slaner School of Graduate Studies

Efficacy optimization of low frequency gas bubble-mediated sonoporation as a drug delivery platform to cancer cells

A thesis submitted toward the degree of

Master of Science in Biomedical Engineering

by

Michal Eck

This research was carried out in the Department of Biomedical Engineering

Under the supervision of Dr. Tali Ilovitsh

Acknowledgments

First, I would like to thank my supervisor Dr. Tali Ilovitsh for the constant guidance and support. I truly appreciate the time devoted for discussions to improve the research and the opportunity to be mentored by her in the academic world.

I would also like to thank Dr. Ramona Aronovich for her guidance and help in planning and executing the experiments, and Mike Bismuth for his assistance in executing the NB experiments.

Also, many thanks to all members of the Ilovitsh lab for the time we spent together and for all of the support and professional discussions.

I would like to dedicate this thesis to my dear family and thank them for their support, love and constant encouragement.

Abstract

Ultrasound insonation of gas bubbles can form pores in cell membranes and facilitate local trans-membrane transport of drugs and genes. An important factor in efficient delivery is the size of the delivered target compared to the generated membrane pores. Large molecule delivery remains a challenge, and can affect the resulting therapeutic outcomes. To facilitate large molecule delivery, large pores need to be formed. While ultrasound typically uses megahertz frequencies, it was recently shown that when microbubbles are excited at a frequency of 250 kHz (an order of magnitude below the resonance frequency of these agents), their oscillations are significantly enhanced as compared to the megahertz range. Here, to promote the delivery of large molecules, we suggest using this low frequency to induce large pore formation through the high-amplitude oscillations of micro- and nano-bubbles. We assessed the impact of low frequency microbubble-mediated sonoporation on breast cancer cell uptake by optimizing the delivery of 4 fluorescent molecules ranging from 1.2 to 70 kDa in size. The optimal ultrasound peak negative pressure was found to be 500 kPa. For molecule sizes of 1.2 and 4 kDa, treatment with 500 kPa and MB resulted in 58% and 29% of fluorescent cells respectively, whereas delivery of 20 kDa and 70 kDa molecules yielded 10% and 5%, respectively. These findings suggest that low-frequency insonation of microbubbles results in high amplitude oscillation in vitro that increase the uptake of large molecules. Next, we sought to develop a non-targeted approach using nanobubbles instead of microbubbles, to facilitate translation to in vivo experiments. We investigated the delivery of 1.2 and 4 kDa fluorescent molecules using nanobubbles and low frequency ultrasound and were able to obtain similar uptake percentage as with microbubbles. We find that successful ultrasound-mediated molecule delivery requires the careful selection of insonation parameters to maximize the therapeutic effect by increasing cell uptake.

Contents

Abbreviations

US……. Ultrasound

MB……..…..…Microbubble

TMB…… Targeted Microbubble

NB……Nanobubble

PNP……..…...…Peak negative pressure

IT……..……...Intratumoral

EPR…….……. Enhanced permeability and retention

MI……...……Mechanical Index

FDA…….....…...Food and Drug Administration

List of figures

List of Publications

- **Michal Eck**, **Ramona Aronovich** and **Tali Ilovitsh**, “Low frequency microbubble-mediated ultrasound as an enhanced drug delivery platform to cancer cells”, International Journal of Pharmaceutics:x, Vol. 4, 100132. (2022).

1 Introduction

For many years ultrasound (US) was mainly known for its diagnostic use, however, there are also many therapeutic applications that can be carried out using US. These applications include lithotripsy, histotripsy, blood brain barrier opening, drug delivery, gene therapy and more [1]. This thesis will focus on drug and gene delivery via a process called sonoporation.

US has many advantages including its non-invasiveness along with deep penetration depth, it is cost-effective and portable, making it very convenient to handle. Here, we focused on the sonoporation process as a way to delivery different sized materials into cancer cells and enhancing the process with the addition of either free microbubbles (MB), targeted MB (TMB) or free nanobubbles (NB).

This thesis examined the relationships between different parameters in the designed experiment system, including US parameters used, such as frequency and peak negative pressure (PNP), the delivered material size, the bubble size and the effect of specifically targeting the MB to the cell surface compared to free MB. In contrast to previous studies that examined the sonoporation process with frequencies above 1 MHz, here we investigated the effect of low frequency (i.e., 250 kHz) on the delivery of molecules with different molecular weights. Low frequency enables high amplitude oscillations of the MBs and as a result the creation of large pores in adjacent cell membrane. Thus, by using low frequency sonoporation we were able to facilitate delivery of large molecules and to optimized the sonoporation efficacy with regards to insonation parameters and the delivered molecule size in the same experimental setup. Low frequency MB-mediated ultrasound can serve as an effective drug delivery platform of large molecules with high spatiotemporal precision.

At first, a MB dynamic under US field simulation was performed to study the MB behavior and to better choose the desired PNP range. Then, experiments were done starting with TMBs and varying molecule sizes from a small 1.2 kDa fluorescent dye material to 70 kDa material, to investigate the dependence between molecule size and cell uptake efficacy under low frequency ultrasound application. To facilitate the creation of the pores in the cell membrane and delivery of material into the cells the MBs are required to be in proximity of the cells. Due to the MBs size, to achieve this requirement in-vivo, an intratumoral (IT) injection should be used. This may be problematic if the tumor is located in a difficult to reach area. To overcome this obstacle, in the second stage of the project, NBs were developed as a non-invasive alternative to MBs. Due to their smaller size, 200 nm NBs can be injected systemically and accumulate at the tumor site via the enhanced permeability and retention (EPR) effect. As the tumor vessels are more permeable, the NBs can pass through the leaky vessels and accumulate at the tumor. However, the NBs response to US is considered limited. Due to their small size NBs are usually being used with high frequency US that correlate with the order of their resonance frequency [2]–[4]. At those frequencies, high-amplitude oscillations were not observed [5]. Due to the MBs limitation described previously, we decided to investigate additionally whether the same physical effect that causes the MBs for high-amplitude oscillations under low frequency US can cause a similar reaction with NBs and enable the development of NB-mediated sonoporation using low frequencies.

Cells viability was also measured throughout all of the experiments to understand the correlation between uptake by the cells and their remaining vitality. Background about sonoporation mechanisms, the influence of the frequency used and MBs on efficacy and how it relates to cancer treatment is elaborated in chapter 3. Chapter 4 describes the methods

used in the research and the materials preparations. The results are presented in chapter 5 and further discussed in chapter 6. Conclusions and future work are discussed in chapter 7.

2 Research objectives

The main objective of this work was to assess the impact of low frequency gas bubbles-mediated sonoporation on breast cancer cell uptake by optimizing the delivery of four molecules ranging from 1.2 kDa to 70 kDa using 250 kHz center frequency. At a first step, we developed a method for TMB-mediated sonoporation to enhance molecules delivery into the cells. Then, an improved method was developed by using free NBs instead of TMBs. In addition, an assessment of cells viability post treatment was also performed. This optimization along with an understanding of the relationship between the different parameters can advance this therapeutic platform of MB and NB-mediated sonoporation and could be used in the future as a combined method to maximize the therapeutic effects of cancer treatment.

The first step was to simulate the MB response to various US parameters and understand how the expansion ratio is affected by it. The MB dimensions were similar to the MB prepared to be used in the experiments. Next, uptake analysis was performed for the different molecule sizes along with viability assessment. Then, experiments using free MB and free NB were carried out and the results were compared to the TMB experiments.

3 Background

3.1 Therapeutic US applications

In contrast to diagnostic US, which is mostly a passive imaging method used to study and identify anatomy and structures within the body and to provide information on how to address different conditions, therapeutic US aims to actively change the tissues ordinary functions and status to treat numerous conditions by inducing biological effects [1]. Therapeutic US can be used in many areas of the body such as the brain, kidneys, skin and more. Some of the methods being explored consist of heating, mechanical stress and permeabilization.

For example, when ultrasonic energy is absorbed by the body's tissues it is converted into heat and results in tissue heating to a certain extent. By focusing the ultrasonic beams the heat is intensified at a specific spot and can lead to thermal ablation at a targeted tissue [6].

Also, when combined with a cavitation nuclei, such as MBs, focused high pressure short pulses US can, for example, induce histotripsy and mechanically destroy a solid tumor [7].

With US advantages to penetrate through the skull, along with cavitation induced effects, permeabilization of the BBB can be achieved. BBB opening enables drugs delivery (e.g. cancer and Alzheimer treatments) to the brain, a path that is typically blocked [1].

The ultrasonic permeability effect can enhance drug and gene delivery not only to the brain, but also to many regions of the body, specifically to cancer tumors located at different organs. To enhance membrane permeability and to enable delivery to the cells a method called sonoporation can be used. In sonoporation, US waves generate cavitation to induce

pores in cell membranes, enabling the surrounding material (e.g., drugs, genes) to enter the cell through these temporary open pores.

Other cell delivery mechanisms exist such as viral vectors and electroporation. Viral vectors are associated with relatively high transfection efficacy; however, the risk of viral infection and cytotoxicity are critical disadvantages. Electroporation, which is a non-viral method, has the advantage of low infection risk and decreased host immunogenicity response, however, its efficacy is much lower than viral vectors methods [8], [9].

Sonoporation can provide a solution for drug and gene delivery into cells without the viral vectors risks and with improved efficacy compared to electroporation.

3.2 MB and NB

Most sonoporation methods utilize MB contrast agents to increase the sonoporation efficacy [10]. MBs are spherical and are composed of a gas core and a stabilizing shell. Upon US application, the MB acts as a cavitation nuclei that enhances mechanical bioeffects, including membrane permeabilization [2], [3]. MB expand when the US pressure is negative and contract when it is positive (Fig. 1). This results in MB oscillations throughout the positive and negative phases of the US wave, which affect their surroundings. When close to cells, these oscillations disrupt the integrity of the cell membrane, which is resealed after US activation is halted [11].

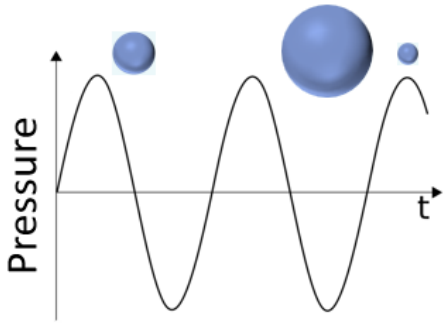

Figure 1 - MB oscillations under US pressure. MB expand under the negative pressure phase and contract at positive pressure phase.

This process forms transient pores in cell membranes that enable the delivery of non-permeable extracellular molecules including drugs, proteins, genes and a variety of therapeutic agents [4]. The use of cell-targeted MB further enhances the sonoporation effect, since the close proximity between the adherent MB and the cell surface improves the efficacy of pore creation [5], [6]. Upon US excitation, MBs oscillate, thus increasing cell membrane permeability and providing a conduit for the delivery of different therapeutics into the target region (Fig. 2).

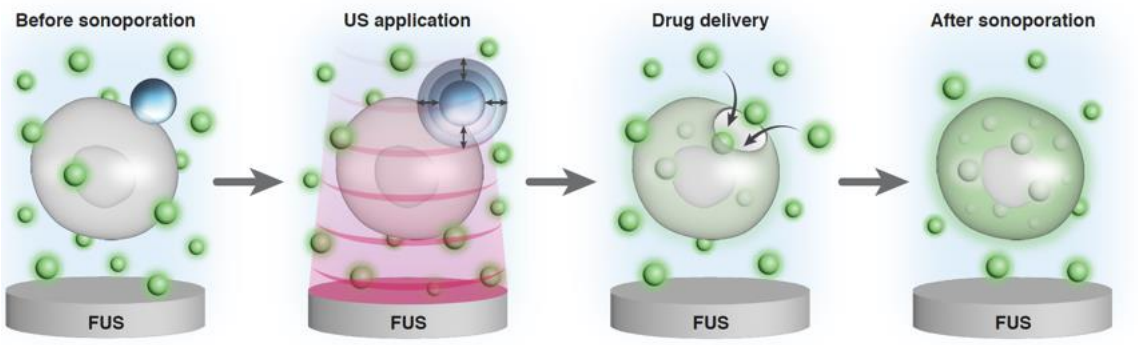

Figure 2 - MB-mediated sonoporation process. Upon US activation the MB begin to oscillate and form transient pores in cell membrane, enabling the delivery of non-permeable extracellular molecules. When US application stops the membrane is resealed and the material remains trapped inside the cell.

Sub-micron bubbles, known as NBs, are another class of contrast agents. NBs are also composed of a gas core and a stabilizing shell and the same cavitation effects induced by MBs can be achieved using NBs [12]. However, their obtained bioeffects were considered limited as a result of their small size, when high frequency insonation was used. Here, we sought to evaluate the NB response to low frequency insonation and optimize their bioeffects for cell pores formation. The NBs main advantage is their ability to move more freely within capillaries, and their accumulation in tumors via the EPR effect. These advantages could be used in the future for noninvasive tumor therapy.

3.3 Stable and inertial cavitation

MB oscillations depend on the applied PNP. At low PNPs, the MBs expand and contract at relatively small amplitudes around an equilibrium value. These low amplitude oscillations are considered as stable cavitation. During stable cavitation, sonoporation can occur via biophysical effects such as pushing and pulling the cell membrane during MB expansion

and contraction or by affecting the liquid movement in the MB area, known as microstreaming, which results in applied shear stress to the cells membrane [10], [13].

When a certain pressure threshold has been reached, inertial cavitation initiates. During inertial cavitation, there is a significant MB expansion, leading to MB collapse and fragmentation, which can result in a more aggressive biophysical effect such as a violent shock wave or liquid jetting that can cause membrane perforation [10], [14], [15].

To measure the MB response and to distinguish between stable and inertial cavitation we can use numerical simulations that predict the MB expansion ratio, which is the maximal diameter of the MB, at its expansion phase, divided by the initial resting diameter. Stable cavitation is defined for expansion ratios from 1.1 to 3.5. Beyond an expansion ratio of 3.5 fold, inertial cavitation begins [14].

3.4 Marmottant model

An understanding of how MBs, or other UCA, act under an US field is required to better utilize them for various applications at different ultrasonic field conditions. The experiments included in this thesis were done with gas filled MBs with a lipid shell, so a model that best describes this type of MBs was needed. A well-known model is based on the Rayleigh-Plesset equation for a free gas bubble in an incompressible fluid:

$$\ddot{R}R + \frac{3\dot{R}^2}{2} = \frac{1}{\rho_l}\left(P_l - \frac{4\mu\dot{R}}{R} - P_{ac}(t)\right) \qquad (1)$$

In this equation R(t) represents the dynamic radius of the bubble over time, ρ_l is the liquid density, P_l is the liquid pressure close to the bubble wall, μ is the liquid viscosity and P_{ac} is the acoustic pressure over time. Over the years, more advanced methods have developed.

These methods take into account additional parameters such as the lipid shell parameters, which is a crucial part as this lipid coating changes the effective surface tension and affects the bubble dynamics considerably due to its increase of mechanical stiffness and sound damping [1], [16]. A very popular model is the Matmottant model, proposed by Philippe Marmottant et al. which takes into consideration the lipid coating of the MB and its asymmetric oscillations due to the large variations of the surface area [16]. The three main parameters taken into account in this model are: a buckling surface radius, a shell compressibility, and a break up shell tension. Therefore, this model is based on three linear regimes that depend on the bubble area A:

$$A = 4\pi R^2 \qquad (2)$$

There are three main states for the bubble, with the first one being a buckled state, for which the surface tension, σ, is 0 due to the compression of the bubble and the phospholipid shell arrangement at this state. Meaning, for $R \leq R_{buckling}$:

$$\sigma = 0 \qquad (3)$$

The second state is the elastic state, with an elastic modulus χ. In the range of bubble radius $R_{buckling} \leq R \leq R_{break-up}$:

$$\sigma = \chi\left(\frac{A}{A_{buckling}} - 1\right) = \chi\left(\frac{R^2}{R_{buckling}{}^2} - 1\right) \qquad (4)$$

The third state is a ruptured state in which due to a fast expansion of the bubble, the shell breaks at a certain tension, $\sigma_{break-up}$. At this state the surface tension of the bubble will be the same as the surrounding liquid, water in this case, thus for $R_{break-up} \leq R$:

$$\sigma = \sigma_{water} \qquad (5)$$

The Marmottant model for bubble dynamics combines the Rayleigh-Plesset equation and the following polytropic gas law with surface tension dependance on the bubble changing radius:

$$P_g(t) - P_l(t) = \frac{2\sigma(R)}{R} + 4\mu\frac{\dot{R}}{R} + 4\kappa_s\frac{\dot{R}}{R^2} \qquad (6)$$

Where P_g is the gas pressure in the bubble, P_l is the liquid pressure, R is the bubble radius, $\sigma(R)$ is the bubble surface tension as a function of the bubble radius, μ is the liquid viscosity, and κ_s is the surface dilatational viscosity from the monolayer.

Therefore, the final Marmottant model equation for bubble dynamics is:

$$\rho_l\left(R\ddot{R} + \frac{3}{2}\dot{R}^2\right) = \left[P_0 + \frac{2\sigma(R)}{R_0}\right]\left(\frac{R}{R_0}\right)^{-3\kappa}\left(1 - \frac{3\kappa}{c}\dot{R}\right) - P_0 - \frac{2\sigma(R)}{R} - \frac{4\mu\dot{R}}{R} - \frac{4\kappa_s\dot{R}}{R^2} - P_{ac}(t) \qquad (7)$$

Where P_0 is the ambient pressure, R_0 is the equilibrium radius of the bubble, κ is the polytropic gas exponent, c is the sound velocity in the liquid, and P_{ac} is the acoustic pressure [16].

3.5 Low-frequency sonoporation

Sonoporation efficacy depends on the cell type, the size of the generated pore, and the delivered particle size, among other parameters. The pore size is affected by factors such as the MB concentration, formulation, targeting method, treatment duration, and US parameters [17], [13]. These parameters also affect the duration of the opened pore and the end result of successful delivery or cell death [18], [19]. Enlarging the pores by enhanced MB oscillations is likely to increase cellular uptake via sonoporation.

Earlier works assumed that MB oscillations are enhanced at their resonance frequency [20]. The resonance frequency depends on factors such as the MB diameter, composition and

surrounding medium [21], and is typically above 1 MHz [4]. For these reasons, MB-mediated sonoporation optimization studies applied insonation at frequencies of 500 kHz and above, although most were above 1 MHz [22]–[26]. However, more recent studies have shown that at a low frequency of 250 kHz, which is an order of magnitude below the MB resonance frequency, enhanced MB oscillations are observed and can increase sonoporation efficacy [14], [27]. The physical mechanism accounting for this phenomenon is known as the Blake threshold effect, which states that when exciting a MB well below its resonance frequency, beyond a defined threshold pressure (Blake threshold), the MB will expand extensively [28]–[30]. These high amplitude oscillations can transform the TMB into mechanical therapeutic warheads that poke large holes in cell membranes. This effect was recently shown to facilitate the delivery of large genes into cancer cells [27], and for low energy mechanical ablation of tumors [7], [31].

Figure 3 simulates the MB expansion ratio for an initial resting diameter of 1.5 μm for center frequencies of 250 kHz in green and 1 MHz in red. For the low frequency of 250 kHz, we can see a much higher expansion ratio when compared to 1 MHz for pressures above 200 kPa. This high expansion ratio shows that for 250 kHz inertial cavitation initiates around 200 kPa, which is a relatively low pressure, meaning that we can expect a more robust sonoporation effect at lower pressures with 250 kHz when compared to 1 MHz.

In order to deliver large particles using sonoporation, we need large pores in the cell membrane. The large pores can be created by high MB expansion ratio which is achieved at low frequencies.

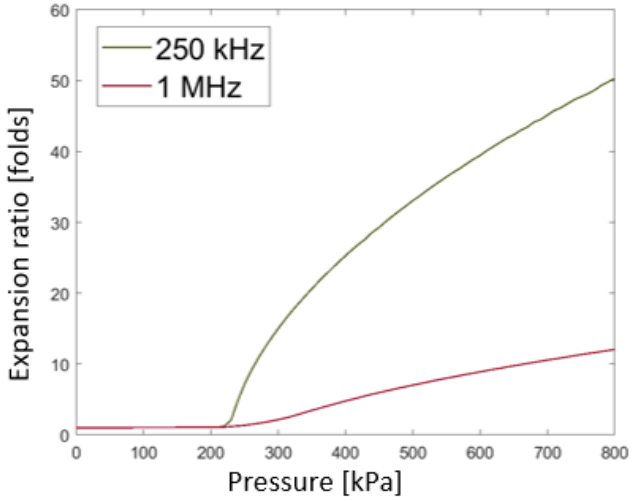

Figure 3 - Expansion ratio simulation. MB expansion ratio for an initial resting diameter of 1.5 μm for center frequencies of 250 kHz in green and 1 MHz in red.

Given the advantages of low frequency insonation, and the growing interest in the use of low frequencies [27], [32], [33], there is a crucial need for studies on ways to optimize the relationship between molecule size and delivery efficacy upon low frequency sonoporation for effective drug delivery. This study assessed the impact of particle size on cell uptake by directly comparing the delivery of 4 molecules with different molecular weights. Most previous sonoporation studies have examined the delivery of small molecules such as Propidium Iodide (PI) [34]–[40]; however, the delivery of small molecules does not fully represent the ability to deliver larger particles. Hence, this study examined the sonoporation effect on molecules ranging from 1.2 kDa up to 70 kDa. This size range corresponds to materials such as chemotherapeutic drugs and drug carriers (1-70 kDa), siRNA (~14kDa) and proteins (3-40 kDa) [16], [41]–[49].

Further, as seen in the simulation, the use of a low frequency reduces the pressure needed to achieve effective delivery. As a result, the spatiotemporal precision of the method is improved, since only the MBs and the target tissues are affected, while the healthy

surrounding tissue remains unaffected. Moreover, the low energies do not induce heat, so that the effect remains purely mechanical. The additional benefits of the use of low frequency have to do with its large penetration depth as a result of low attenuation compared to high frequencies, which is likely to facilitate the treatment of deep-seated tissues and organs.

3.6 Mechanical Index

US is considered a safe method relying on over 60 years of use, mostly for diagnostics. It is non-invasive and does not emit ionizing radiation. Still, as a result of US waves interaction with tissues in the body, bioeffects such as thermal and mechanical effects can occur and are even desired at a certain extent for some applications. An important distinction should be done between reversible and irreversible bioeffects and an understanding of the intended outcome, as a result of the US induced bioeffects, is needed in order to avoid harm.

As mentioned, the two main types of bioeffects are heating and cavitation and for each one a calculated index was defined to better evaluate the effect [1].

The thermal index for soft tissues is defined as:

$$\mathrm{TIS} = \frac{\mathrm{W}_0 \cdot f[MHz]}{210[\mathrm{mW} \cdot \mathrm{MHz}]} \qquad (8)$$

Where W_0 is the time-averaged acoustic power and f is the frequency in MHz.

Due to the use of MBs and the exploitation of their cavitation effect, the significant index here is the mechanical index (MI), as it is related to cavitation-induced mechanical effects and defined as:

$$MI = \frac{PNP\ [MPa]}{\sqrt{f[MHz]}} \qquad (9)$$

The Food and Drug Administration (FDA) limit for MI is 1.9 and this limitation guided us when choosing the US parameters in the experiments presented in this thesis. Usually, the mechanical index range for sonoporation is between 0.2 to 1.9 [21].

3.7 Cancer treatment

The main focus here centers on breast cancer cell sonoporation. Their sonoporation is often more challenging than other cell types, such as muscle cells where small MB oscillations suffice for robust sonoporation [46]. In addition, drug delivery to cancer cells has a high clinical importance. Currently, cancer treatment involves invasive surgery combined with adjuvant therapy such as chemo- or immuno-therapy. However, the lack of specificity of these adjuvant therapies and their toxic nature triggers systemic toxic side effects in healthy tissues [47]. By contrast, TMB-mediated sonoporation is a site specific targeted delivery method [15], [48]. Moreover, reducing tumor burden plays a key role in the success of adjuvant therapies [49]. Along with enhancing drug delivery, low frequency insonation of MBs can reduce cancer cell viability, as a combined strategy for cancer treatment.

3.8 NB sonoporation

Many of the sonoporation methods use UAC such as MB to enhance the sonoporation efficacy due to the initiation of the sonoporation effect at lower pressure when compared to sonoporation without MBs. However, in addition to MBs, the efficacy can also be enhanced with reducing of the bubbles size to nano dimensions, meaning NBs. With their smaller size, NBs have an advantage over MBs as they can better pass small vessels, such as the capillary bed, without the fear of blocking them and they can accumulate at the tumor site due to the

EPR effect [50],[51]. The EPR effect, meaning the enhanced permeability of the tumor, is caused due to a rapid and unorganized growth of vasculature and hindered lymphatic removal paths. NB, or other nano sized particles, can more easily pass through these permeable vessels and accumulate at the tumor, in contrast to healthy tissues in which the arranged vasculature system does not enable it [52]. For MB-mediated sonoporation the MB need to be injected intratumorally to be close to the tumor cells, and it might be problematic depending on the tumor location. Therefore, NBs have an advantage with the ability to reach tumors via systemic administration.

Another advantage that NBs have over MBs is their movement in suspension. To achieve the MB-cell proximity required for the sonoporation effect, cell-targeted MBs are needed since MBs immediately float in a suspension. If the MBs are not linked to the cell surface, the MBs will float to the top of the suspension away from the cells. However, by using cell-targeted MBs we enforce their vicinity. NBs behavior in a suspension is different as they are more neutrally buoyant in a Brownian motion in the suspension, allowing them to stay close to the cells for a longer duration [12]. Therefore, when using NBs, a targeting method is not needed and free NBs can be used. This is another advantage of NBs over MBs as it simplifies the preparation process.

As for sonoporation studies with MBs, for NBs also most of the studies employed frequencies of 1 MHz and above [50], [51], [53]–[59], still, due to the low frequency advantages of sonoporation with MB, an understanding of the sonoporation efficacy with NB at low frequencies is also needed. Sonoporation experiments with NBs were also done as part of this thesis and outcome was compared to sonoporation with MBs.

4 Materials and methods

4.1 Numerical modeling

The MB expansion ratio was estimated using the Marmottant model [16] which exhibits good fit with experimental observations [14], [60]. The simulation was implemented in Matlab (version 2017b, The MathWorks, Natick, MA, USA), and took the MB composition, the viscosity and density of the surrounding medium, and the US excitation parameters into account. The MB expansion ratio, defined as the maximal diameter divided by the resting MB diameter, was evaluated for a center frequency of 250 kHz and PNPs ranging from 0 to 800 kPa. The simulation parameters were described previously [31]. The initial MB resting diameter was set to 1.5 μm.

4.2 Microbubble preparation

TMBs composed of a phospholipid shell and a perfluorobutane (C4F10) gas core were used in this study and prepared as reported previously [27]. Briefly, for the TMB preparation, the following lipids (2.5 mg per 1 mL) were combined in a 90:5:5 molar ratio: distearoylphosphatidylcholine (DSPC), 1,2-distearoyl-sn-glycero-3-phosphoethanolamine-N- [methoxy(polyethylene glycol)-2000] (ammonium salt) (DSPE-PEG2K), and 1,2-distearoylsnglycero- 3-phosphoethanolamine-N-[biotinyl(polyethylene glycol)2000] (DSPE-PEG2000-Biotin). All lipids were purchased from Sigma-Aldrich. The lipids were sonicated at 62°C with a 7.4 pH buffer solution (80% NaCl, 10% glycerol, and 10% propylene glycol) and aliquoted into vials (1 mL in each). After sealing the vial, the air within the 1 ml gap in the vial was replaced by perfluorobutane gas. This was done by inserting a perfluorobutane gas syringe with a 21G needle into the vial, and slowly purging

it inside. In parallel, 27G needle was inserted through the rubber cap, into the top of the vial. This needle was used as an outlet for the excess air and perfluorobutane gas. The vials were kept at 4°C until use. Upon use, to activate the TMB, the vial was shaken for 45 seconds in a VIALMIX shaker. Then, using centrifugation, the TMB were purified by removing most of the TMBs with radii smaller than 0.5 μm. 400 μg of streptavidin (Thermo Fisher Scientific, S888) was added to the TMB which were then incubated on a rotator for 25 minutes. After the 25- minute incubation period the TMB were purified again using centrifugation to remove excess streptavidin. Then, 15 μg of Biotin anti-mouse CD326 antibody (EpCAM, BLG-118204) was added to the TMB, which were incubated again on a rotator for 25 minutes and then purified in the same way to remove the excess antibody. Figure 4 shows a syringe with TMB after purification. The TMB size and concentration were measured using a particle counter system (AccuSizer FX-Nano, Particle Sizing Systems, Entegris, MA, USA).

The amount of streptavidin and CD326 antibody per TMB was estimated as follows: the DSPC headgroup has an average area of 0.6 nm2 [27], [61], [62]; thus, a MB with an average diameter of 1.5 μm has ~10^7 lipid molecules/shell [$\pi*(1.5*10^{-6})^2/(0.6*10^{-18}) \cong 10^7$]. 5% of the total lipids are DSPE-PEG-Biotin; therefore, each MB has $5*10^5$ DSPE-PEG2K-Biotin. We assume that one biotin-lipid conjugates with one streptavidin and therefore each MB has ~$5*10^5$ streptavidin. On average, assuming that two antibody molecules bind to one streptavidin, each TMB has ~$10*10^5$ antibody molecules [63].

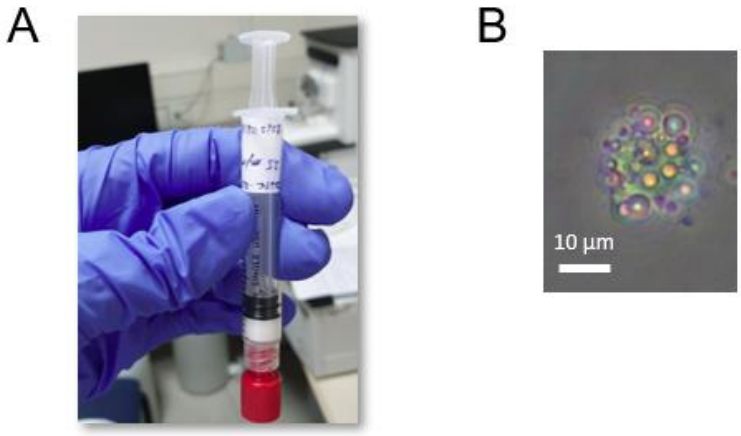

Figure 4 – Microbubbles. (A) Syringe with TMB before adding it to the cell suspension. (B) A microscope image showing a cell with TMBs attached to the cell, at 20X magnification.

4.3 Nanobubbles preparation

For NB preparation 1,2-dibehenoyl-sn-glycero-3-phosphocholine (C22, Avanti Polar Lipids Inc., Pelham, AL), 1,2-dipalmitoyl-sn-glycero-3phosphate (DPPA, Corden Pharma, Switzerland), 1,2-dipalmitoyl-sn-glycero-3-phosphoethanolamine (DPPE, Corden Pharma, Switzerland), and 1,2-distearoyl-snglycero-3-phosphoethanolamine-N-[methoxy(polyethylene glycol)-2000] (ammonium salt) (DSPE-mPEG 2000, Laysan Lipids, Arab, AL) were dissolved at 80°C in propylene glycol (PG, Sigma Aldrich, Milwaukee, WI) and sonicated until all lipids were dissolved. Then, the solution was sonicated at room temperature for 10 minutes with an addition of glycerol (Gly, Acros Organics) and phosphate buffer solution (0.8 mL, Gibco, pH 7.4) mixture that was preheated to 80°C. 1 ml of the final solution was aliquoted into each vial and octafluoropropane (C3F8, Electronic Fluorocarbons, LLC, PA) gas was injected into each vial to replace the air.

Upon use, to activate the NB, the vial was shaken for 45 seconds in a VIALMIX shaker and then placed inverted in centrifuge for 5 minutes at 50 rcf to isolate the NB. Using a 21 G

needle, 100 µL of the NB solution was drawn from the vial, taken 5 mm from the bottom of the vial.

4.4 Cell preparation

4T1 cells, murine tumor-derived cell line (purchased from ATCC), were used in all experiments. The cells were cultured in T75 tissue culture flasks containing RPMI 1640 L-Glutamine (+) with 10% fetal bovine serum (FBS) and 1% penicillin−streptomycin (P/S) at 37°C in a humidified 5% CO2 incubator. Upon use, when cell confluency reached 85%, the cells were dissociated using TrypLE Express (Thermo Fisher Scientific, 12604021) and resuspended at a concentration of 2×10^6 cells in 300 µL degassed PBS (calcium (+), magnesium (+)).

4.5 Ultrasound set-up

For the US treatment, a 0.5 mL Eppendorf tube with cell suspension was positioned at the focal spot of a spherically focused single-element transducer (H115, Sonic Concepts, Bothell, WA, USA), which was placed facing upward at the bottom of a degassed water tank (Fig. 5). The transducer was focused to a distance of 45 mm. Each tube was insonated at a center frequency of 250 kHz and PNP that ranged from 100 to 800 kPa for a duration of 30 seconds.

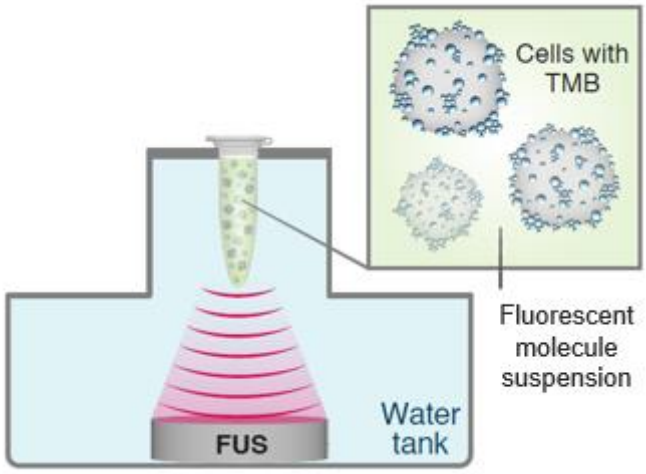

Figure 5 - Microbubble-mediated sonoporation setup. An ultrasound transducer is placed at the bottom of a water tank and a tube containing cells with TMB in a fluorescent molecule suspension is placed at the transducer's focal spot.

4.6 Sonoporation experiments

4.6.1 TMB Sonoporation

Fluorescent molecules ranging from 1.2 kDa to 70 kDa were used to investigate delivery to the cells. Each experiment included one of the following materials: 7-aminoactinomycin D (7-AAD), a 1270 molecular weight (mol wt) fluorescent dye that undergoes a spectral shift upon association with DNA (Thermo Fisher Scientific, A1310), Fluorescein isothiocyanate–dextran average mol wt 4,000 (FITC-Dextran 4) (46944, Sigma-Aldrich), FITC-Dextran 20 (Sigma-Aldrich, FD20), and FITC-Dextran 70 (Sigma-Aldrich, 46945). After cell preparation, TMB were added to the cell mixture at a ratio of 50 TMB per cell [7] and incubated for 20 minutes at room temperature on a rotator allowing the TMB to bind to the cells. Following incubation, microscopy imaging was used to confirm the TMB binding to the cells (Fig. 6). For the same targeted microbubbles concentration used here, it was

previously found that 19.4 ± 3 TMBs were bound per cell. This is a 38.8 ± 6% effective binding rate [7].

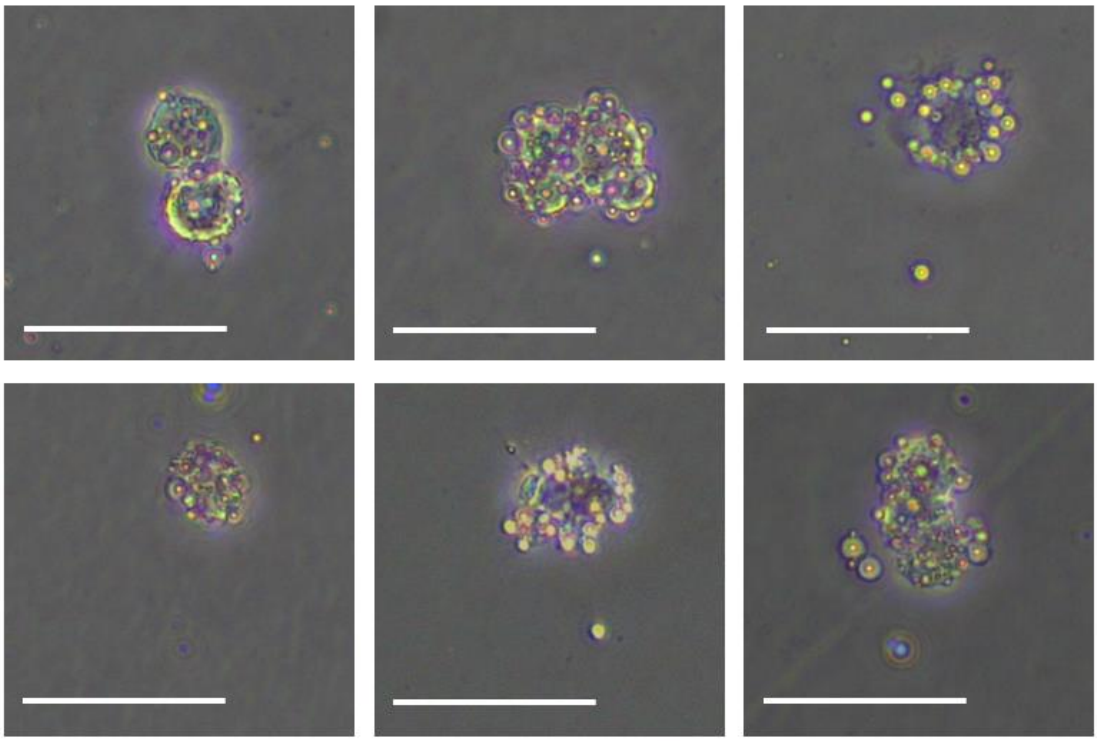

Figure 6 - Cells with targeted microbubbles. Microscope images showing 4T1 cells with targeted microbubbles attached to the cells, at 20X magnification. Scale bar is common to all images and is 50 µm.

For the 7-AAD sonoporation experiments the incubation was performed separately for each group, prior to which the cells were kept on ice. For the FITC sonoporation experiments, the incubation was performed for all groups at the same time.

Following incubation, the mixture of cells and TMB was aliquoted into 0.5 mL Eppendorf tubes, along with degassed PBS +/+ and the sonoporated material (5 µg/ml 7-AAD or 1 mg/ml FITC-dextran). For experiments with 7-AAD and FITC-Dextran 4, due to the molecules' small size, the US treatment was performed immediately after adding the

material to the 0.5 mL Eppendorf tube. For the FITC-Dextran 20 and 70, the cell mixture was incubated for 30 minutes with the materials prior to US treatment .

For the 7-AAD sonoporation experiments, following US treatment, 10 µg/ml of Hoechst (33342, Abcam) was added to the tube to quantify the total number of cells in the sample. The suspension was transferred from the Eppendorf tube to a 35mm cell culture dish (430165, Corning) and viewed under fluorescence microscope using BF, an mCherry filter and a DAPI filter at 10X magnification. Seven frames from different locations of the culture dish were saved to be analyzed further.

For the FITC-Dextran sonoporation experiments, following US treatment, the suspension was transferred from the Eppendorf tube to a 24-well plate (3526, Corning) which was pre-prepared with 300 µl of culture media with an additional 1.5% P/S and then incubated for 24 hours at 37°C in a humidified 5% CO2 incubator.

After incubation for 24 hours, each well was washed 3 times with PBS to remove the remaining FITC suspension and then media were added to each well. Imaging and quantification of the fraction of fluorescent cells was performed using IncuCyte Live-Cell Analysis System (Essen Bioscience). All experiments were performed in triplicate for each group.

4.6.2 Free MB and NB Sonoporation

Fluorescent dye uptake by the cells was calculated for molecules in different sizes. First, a proof-of-concept experiment was performed with 7-aminoactinomycin D (7-AAD), 1.2 kDa fluorescent dye (Thermo Fisher Scientific, A1310). Free NBs were added to the cell suspension and degassed PBS +/+ in an Eppendorf tube at a ratio of 300,000 NBs per cell. Then, 5 µg/ml of 7-AAD was added to the mixture. Each tube was insonated and following the US treatment 10 µg/ml of Hoechst (33342, Abcam) was added to identify the number of

total cells in the sample. The suspension was then viewed under fluorescence microscope in a 35mm cell culture dish (430165, Corning).

Next, a sonoporation experiment was done with Fluorescein isothiocyanate–dextran average mol wt 4,000 (FITC-Dextran 4 kDa) (46944, Sigma-Aldrich). Same as before, NB were added to the cell suspension with degassed PBS +/+ in an Eppendorf tube a ratio of 300,000 NB per cell and then 1 mg/ml of FITC 4 kDa was added. For the MB groups the ratio was 50 MBs per cell. Following US treatment, the suspension was transferred to a 24-well plate (3526, Corning) with 300ul of culture media and 1.5% P/S. The plate was incubated for 24 hours at 37°C in a humidified 5% CO2 incubator. After incubation, the wells were washed three times with PBS to remove any remaining FITC suspension and then media were added to each well. IncuCyte Live-Cell Analysis System (Essen Bioscience) was used for uptake calculation. Experiments were performed in triplicate for each group.

4.7 Viability experiments

Viability was calculated as the percentage of remaining cells in each group compared to the sham group. For the 7-AAD experiments, viability was measured immediately after US treatment using CellDrop device (DeNovix). For the FITC experiments, viability was measured at 24hrs and at 72hrs post-US treatment. These time points were selected in order to match the time points of the molecules uptake experiments. An additional viability test was performed 72 hours post treatment to evaluate cells recovery as a function of time. Following US treatment, the suspension was transferred from the Eppendorf tube to a 24-well plate (Corning, 3526) or 6-well plate (Corning, 3516), which were pre-prepared with either 300ul or 2ml of culture media with an additional 1.5% P/S and then incubated for 24 hours at 37°C in a humidified 5% CO2 incubator. After 24 hours of incubation, each well was washed with PBS, then dissociated with TrypLE and counted using the CellDrop device

(DeNovix). For the three-day viability test, the FITC suspension was washed after one day and then the cells were incubated with media for the remaining time until count.

4.8 Analysis

For the 7-AAD sonoporation experiments, microscope images were analyzed using ImageJ software. Each image was uploaded to the ImageJ software, the image type was changed to 16-bit, the threshold was adjusted to view the stained cells clearly and the background was removed. Each experiment was conducted in triplicate, and 7 images were acquired in each repetition, for a total of 21 images for each group.

The number of Hoechst-stained cells (Blue) was defined as the total number of cells in the sample. The number of red cells was the number of cells stained with 7-AAD. The fraction of fluorescent cells was calculated as the percentage of 7-AAD stained cells divided by the number of Hoechst-stained cells.

For the FITC sonoporation experiments, the analysis was performed using IncuCyte Live-Cell Analysis System (Essen Bioscience). Each well was sampled 25 times at 20X magnification. The calculation used the green confluence (green cell area) normalized by the phase confluence (total cell area). This required configuring the analysis to distinguish cells and the same fluorescence threshold for all images.

GraphPad Prism 9 software was used for the statistical analysis. P values less than 0.05 were considered significant and were adjusted for multiple comparisons as indicated in the figure captions. The results are presented as the mean ± SD.

5 Results

5.1 Numerical Simulations

The MB expansion ratio provided a metric to assess its vibrational response. Expansion ratios from 1.1 to 3.5 were considered to reflect stable cavitation, while inertial cavitation was defined as initiating at expansion ratios of more than 3.5 fold [14]. The size of the generated pore in the cell membrane also depends on the MB expansion ratio. Therefore, to determine the range of PNP for the operation, numerical simulations of the MB expansion ratio were conducted for a center frequency of 250 kHz as a function of the PNP (0 to 800 kPa) (Fig. 7A). MB oscillations are enhanced at a low frequency of 250 kHz, and therefore the stable cavitation range is narrow [14]. Based on these numerical simulations, the predicted stable cavitation range occurs between 85-205 kPa (Fig. 7B). Above this PNP, a steep increase in the expansion ratio initiated and reached factors of 15, 33, and 50 for a PNP of 300, 500 and 800 kPa, respectively.

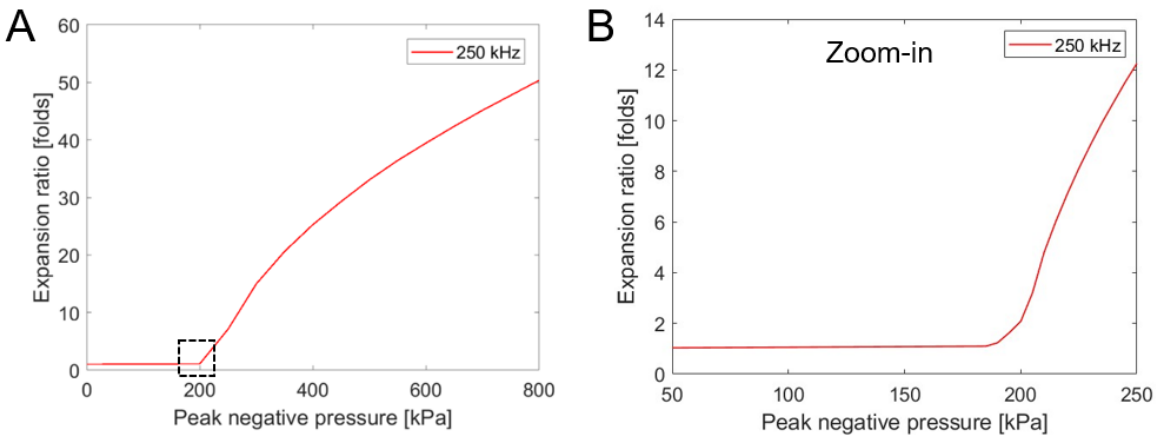

Figure 7 - Predicted MB expansion ratio. Microbubble expansion ratio as a function of the peak negative pressure for 250 kHz and a MB initial diameter of 1.5 µm, for a peak negative range of: (A) 0-800 kPa, and (B) Zoom-in on peak negative pressures of up to 250 kPa.

5.2 Sonoporation results

The delivery of four different sized impermeable dye molecules following low frequency US insonation at a center frequency of 250 kHz was optimized, and directly compared.

5.2.1 TMB-mediated Sonoporation of 7-AAD

The first molecule tested was the 7-AAD, which has a molecular weight of 1.2 kDa. Based on a previous study [64], two 7-AAD concentrations were tested (5 µg/ml and 10 µg/ml), to assess the cell's uptake without US and MB treatment (sham). The fraction of fluorescent cells in the sham group, as observed via fluorescence microscopy, increased as a function of incubation time (Fig. 8A). Therefore, in the following experiments, a time point of 0 (e.g., immediately post-US treatment) was used. For this time point, the fraction of fluorescent cells for both concentrations was similar: 16.8 ± 7.7% for 5 µg/ml and 21.6 ± 3.2% for 10 µg/ml (Fig. 8B). Therefore, a concentration of 5 µg/ml was chosen for the subsequent US and TMB sonoporation experiments.

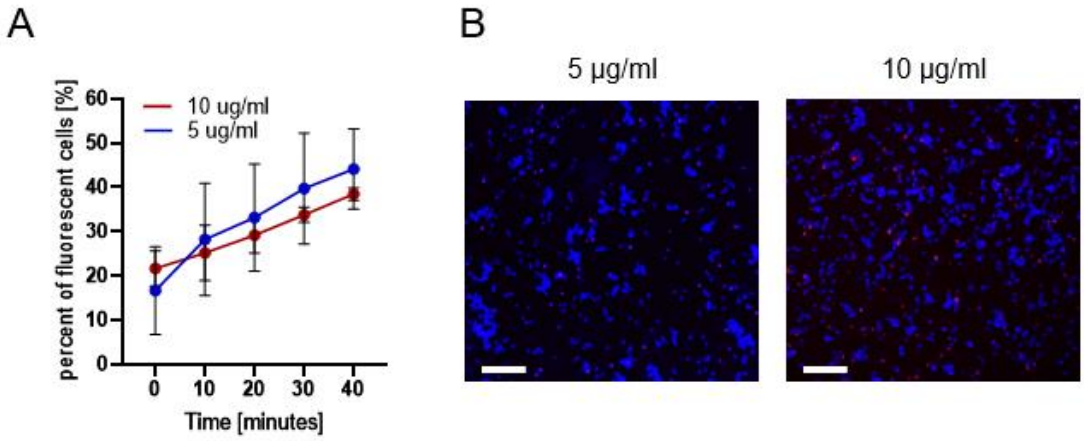

Figure 8 - 7-AAD sham group over time. (A) 7-AAD fluorescent cells as percentage out of total live cells in the sham group over time. (B) Fluorescence microscopy images for the 7-AAD uptake without any treatment (sham) for concentration of 5 µg/ml (left) and 10 µg/ml (right). Scale bar is common to all subfigures in (B) and is 200 µm.

The fraction of 7-AAD stained cells increased as a function of the applied PNP. The percent of fluorescent cells was similar between the sham (21 ± 3%), US only (24 ± 3.3%) and treatment with TMB and US at 100 kPa (21.5 ± 0.9%). The fraction of fluorescent cells reached a maximal value of 57.7 ± 4.9% for 500 kPa (Fig. 9B). Increasing the PNP to 800 kPa reduced the fraction of fluorescent cells to 52 ± 6.3% (non-significant, $p>0.05$). This suggests that 500 kPa was the optimal delivery pressure for this molecule size. The results, presented as folds, increased compared to the sham group and showed a maximal value of 2.8 ± 0.23 fold compared to the sham group (Fig. 9C).

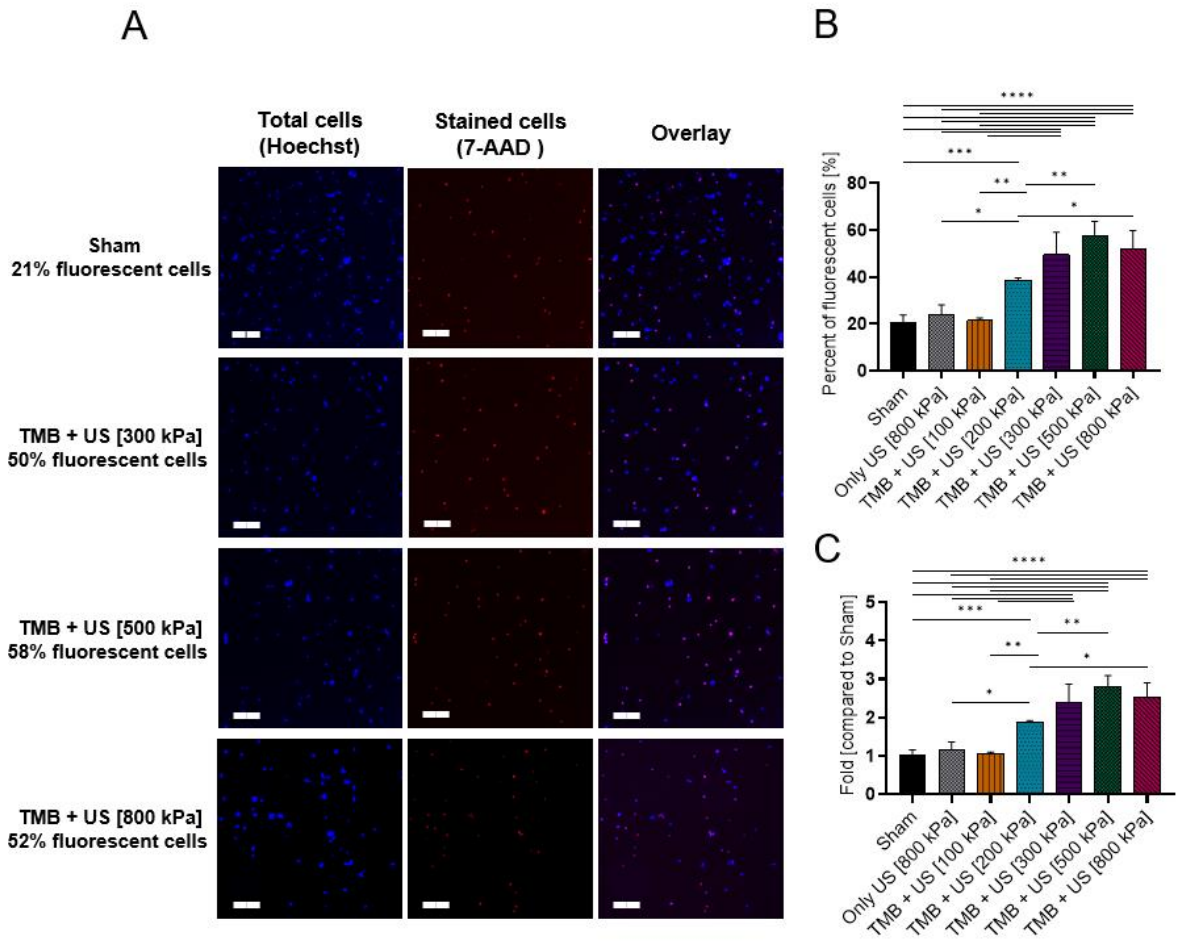

Figure 9 - 7-AAD sonoporation. (A) Fluorescence microscopy images for different ultrasound treatment groups. Each row presents a different PNP immediately following sonoporation. Left column is the Hoechst-stained cells, middle column is the 7-AAD stained cells, and right column is an overlay of both Hoechst and 7-AAD stained cells. Images were acquired with 10x magnification. Scale bar is common to all subfigures in (A) and was 200 µm. (B) 7-AAD stained cells expressed as the percentage of live cells for the different treatment and control groups. (C) The graph in (B) presented as the fold uptake compared to the sham group. (B and C) One-way ANOVA with Tukey's multiple comparison test. Adjusted p values were *p<0.05, **p<0.01, ***p <0.001, ****p <0.0001. All data are plotted as the mean ± SD.

5.2.2 TMB-mediated Sonoporation of FITC 4 kDa

The next molecule that was tested was 4 kDa FITC-dextran. The same FITC-dextran concentration of 1 mg/ml was used for all FITC-dextran sizes (4, 20 and 70 kDa) and was chosen based on previous studies [65]–[68]. FITC 4 kDa exhibited the same delivery trend as 7-AAD, where the fraction of fluorescent cells increased as a function of the applied PNP, up to a PNP of 500 kPa (maximal fraction of fluorescent cells was 29.39 ± 5.07%). Beyond this PNP, the fraction of fluorescent cells began to reduce to 24.14 ± 4.46% for a PNP of 800 kPa (not significant, $p>0.05$) (Fig. 10B). A similar percentage was observed in the control groups of sham (0.77 ± 0.21%) and only US (0.22 ± 0.12%). In addition, the control group of only TMB (2.05 ± 0.86%) had a similar percent of fluorescent cells as the treated group with 100 kPa. These results suggest that 500 kPa was the optimal PNP for the delivery of these molecules, consistent with the 7-AAD results. Specifically, in terms of the fold increase compared to the sham group, the maximal uptake for 500 kPa represented a 38 ± 6.5 fold increase compared to sham group, which was significantly higher than the factor obtained for the 7-AAD molecule (Fig. 10C).

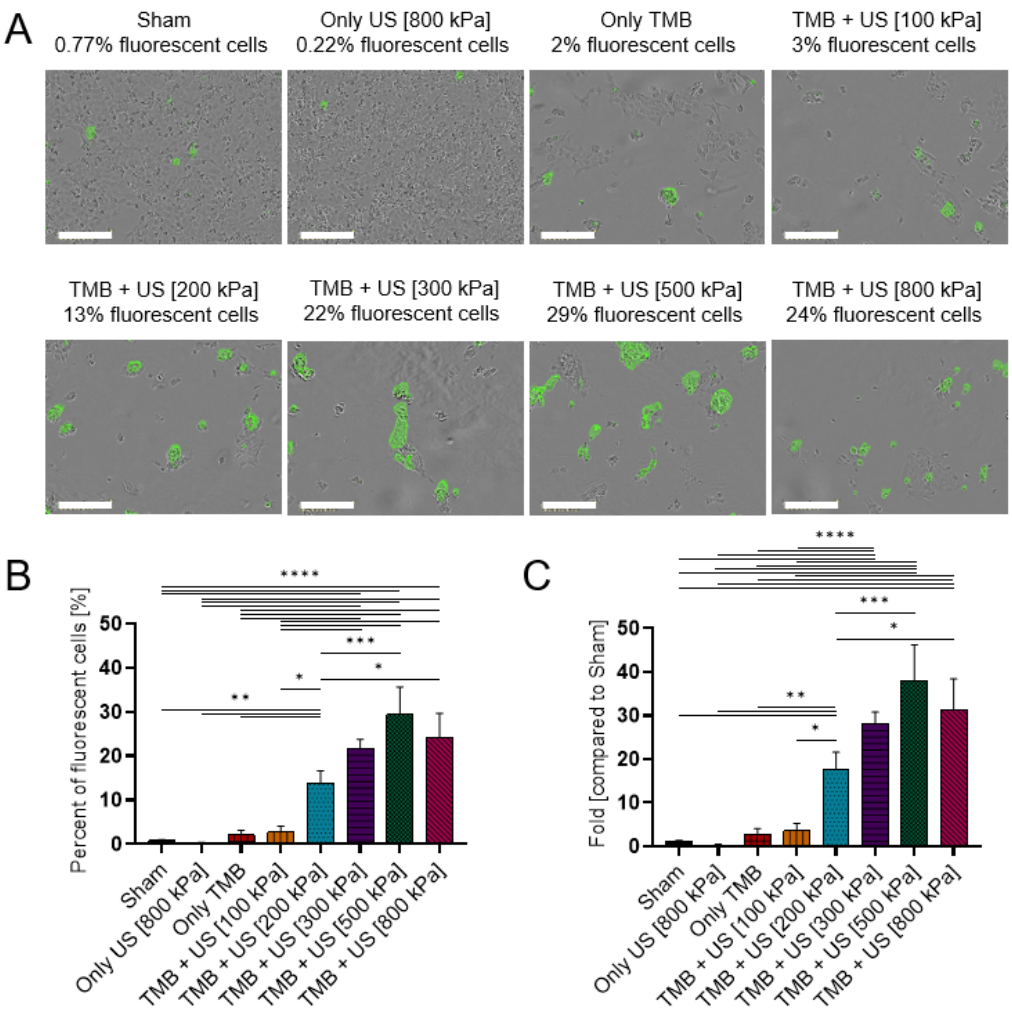

Figure 10 - FITC 4 kDa sonoporation. (A) Overlay images of cells and FITC 4 kDa for different ultrasound treatment groups. Each image presents a different PNP 1 day after sonoporation. Images were acquired by the Incucyte system with 20X magnification. Scale bar is common to all subfigures in (A) and is 200 µm. (B) FITC 4 kDa stained cells expressed as the percentage of live cells for the different treatment and control groups. (C) The graph in (B) presented as fold uptake compared to the sham group. (B and C) One-way ANOVA with Tukey's multiple comparison test. Adjusted p values were *p<0.05, **p<0.01, ***p <0.001, ****p <0.0001. All data are plotted as the mean ± SD.

5.2.3 TMB-mediated Sonoporation of FITC 20 kDa

Next, the size of the delivered molecule was increased to FITC-dextran 20 kDa (Fig. 11). The percent of fluorescent cells increased as a function of the applied PNP. Maximal percentage was observed for a PNP of 800 kPa (13.23 ± 1.32%), while for the 500 kPa the fraction of fluorescent cells was 10.34 ± 1.03% (non- significant, $p>0.05$). A fraction of fluorescent cells of 0.76 ± 0.41% was seen for the sham group and increased for the for the 100 kPa (4.34 ± 1.86%), 200 kPa (5.57 ± 3.01%), and 300 kPa (8.14 ± 1.95%) (Fig. 11B). The maximal fold increase for the 800 kPa PNP compared to the sham group was 17.4 ± 1.74 (Fig. 11C).

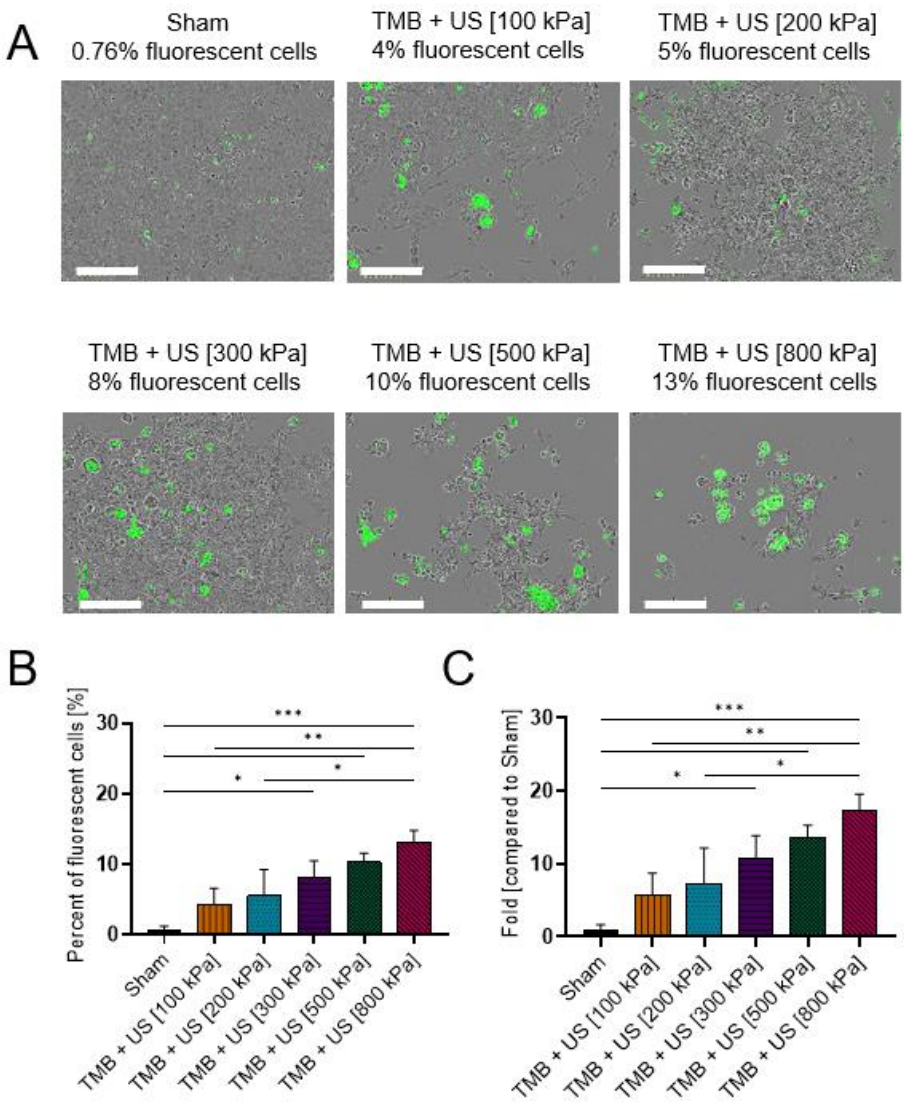

Figure 11 - FITC 20 kDa sonoporation. (A) Overlay images of cells and FITC 20 kDa for different ultrasound treatment groups. Each image presents a different PNP 1 day after sonoporation. Images were acquired by the Incucyte system with 20X magnification. Scale bar is common to all subfigures in (A) and is 200 µm. (B) FITC 20 kDa stained cells expressed as the percentage of live cells for the different treatment and control groups. (C) The graph in (B) presented as fold uptake compared to the sham group. (B and C) One-way ANOVA with Tukey's multiple comparison test. Adjusted p values were *p<0.05, **p<0.01, ***p <0.001, ****p <0.0001. All data are plotted as the mean ± SD.

5.2.4 TMB-mediated Sonoporation of FITC 70 kDa

The largest molecule that was tested was FITC-dextran 70 kDa (Fig. 12). For this molecule size, 0.24 ± 0.03% fluorescent cells was observed in the sham group and 1.4 ± 0.12% for treatment with 100 kPa. A similar percentage was obtained for treatment with 200 kPa (4.22 ± 0.52%) and 300 kPa (4.33 ± 1.19%). Maximal percent of fluorescent cells was observed for 500 kPa (5.3 ± 1.4%) and dropped to 4.32 ± 0.6% for 800 kPa (not significant, $p>0.05$), consistent with the trends observed for the delivery of 7-AAD and FITC 4kDa. The maximal fold increase in uptake for treatment with 500 kPa was 21.5 ± 5.7 compared to the sham group.

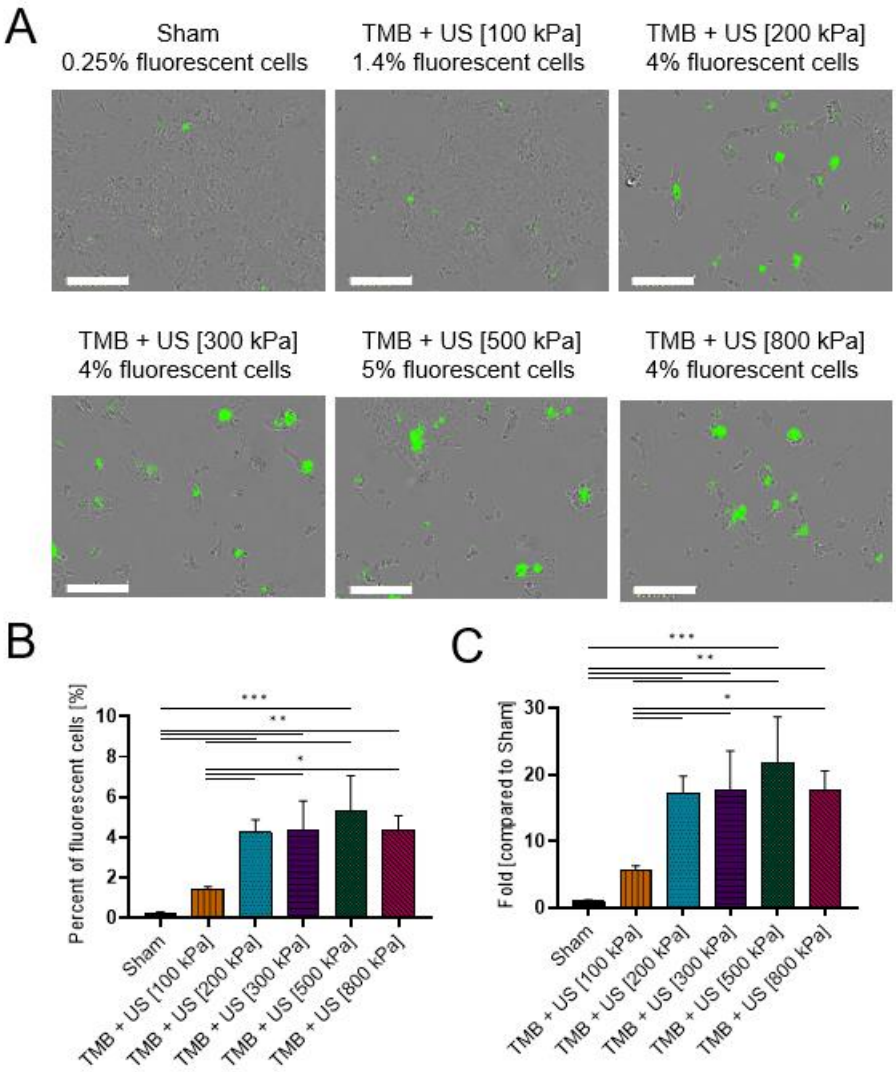

Figure 12 - FITC 70 kDa sonoporation. (A) Overlay images of cells and FITC 70 kDa for different ultrasound treatment groups. Each image presents a different PNP 1 day after sonoporation. Images were acquired by the Incucyte system with 20X magnification. Scale bar is common to all subfigures in (A) and is 200 µm. (B) FITC 70 kDa stained cells expressed as the percentage of live cells for the different treatment and control groups. (C) The graph in (B) presented as fold uptake compared to the sham group. (B and C) One-way ANOVA with Tukey's multiple comparison test. Adjusted p values were *p<0.05, **p<0.01, ***p <0.001, ****p <0.0001. All data are plotted as the mean ± SD.

Uptake percentage was the highest for the smaller molecules and decreased as the molecule size increased (Fig. 13). For PNP of 500 kPa uptake was 58% and 29% for the 1.2 kDa and 4 kDa molecule sizes respectively, while for 20 kDa and 70 kDa it was 10% and 5% repesctively.

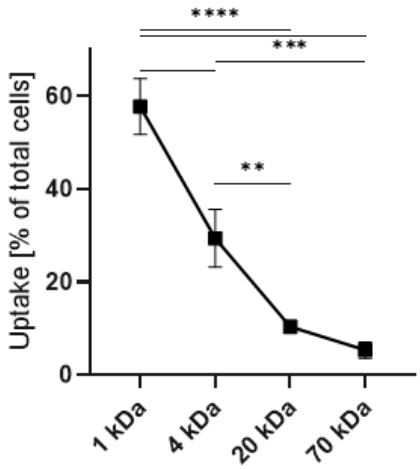

Figure 13 - Uptake at 500 kPa. Uptake expressed as the percentage of live cells for the different molecule sizeses at 250 kHz and 500 kPa PNP. One-way ANOVA with Tukey's multiple comparison test. Adjusted p values were *p<0.05, **p<0.01, ***p <0.001, ****p <0.0001. All data are plotted as the mean ± SD.

5.2.5 Free NB and free MB Sonoporation

5.2.5.1 NB-mediated sonoporation with 7-AAD

NB-mediated sonoporation was initially tested with 7-AAD. Treatment groups were treated with free NB. Treatment with NB only (without US insonation) did not show an increase in uptake compared to the Sham group. Then, treatment with center frequency of 250 kHz and PNP of 800 kPa was performed (MI = 1.6). This pressure was the maximal pressure in the TMB sonoporation experiments, for which 52% uptake was received. Here, with the free NB we saw 61% uptake at 800 kPa. In addition, the total number of cells in the sample did not seem to decrease as much as we saw for the TMB experiments so we decided to increase the PNP to 1350 kPa at 250 kHz (MI = 2.7) to see whether a decrease in cell viability will be seen. At 1350 kPa we still did not see a significant decrease in cells viability immediately after US treatment and uptake was also 61%. Next, based on previous experiments done with free NB, which showed reduced viability of cells at a center frequency of 80 kHz, cells were insonated at 80 kHz and 360 kPa (MI = 1.27), which showed 70% uptake. Results are presented in Fig. 14.

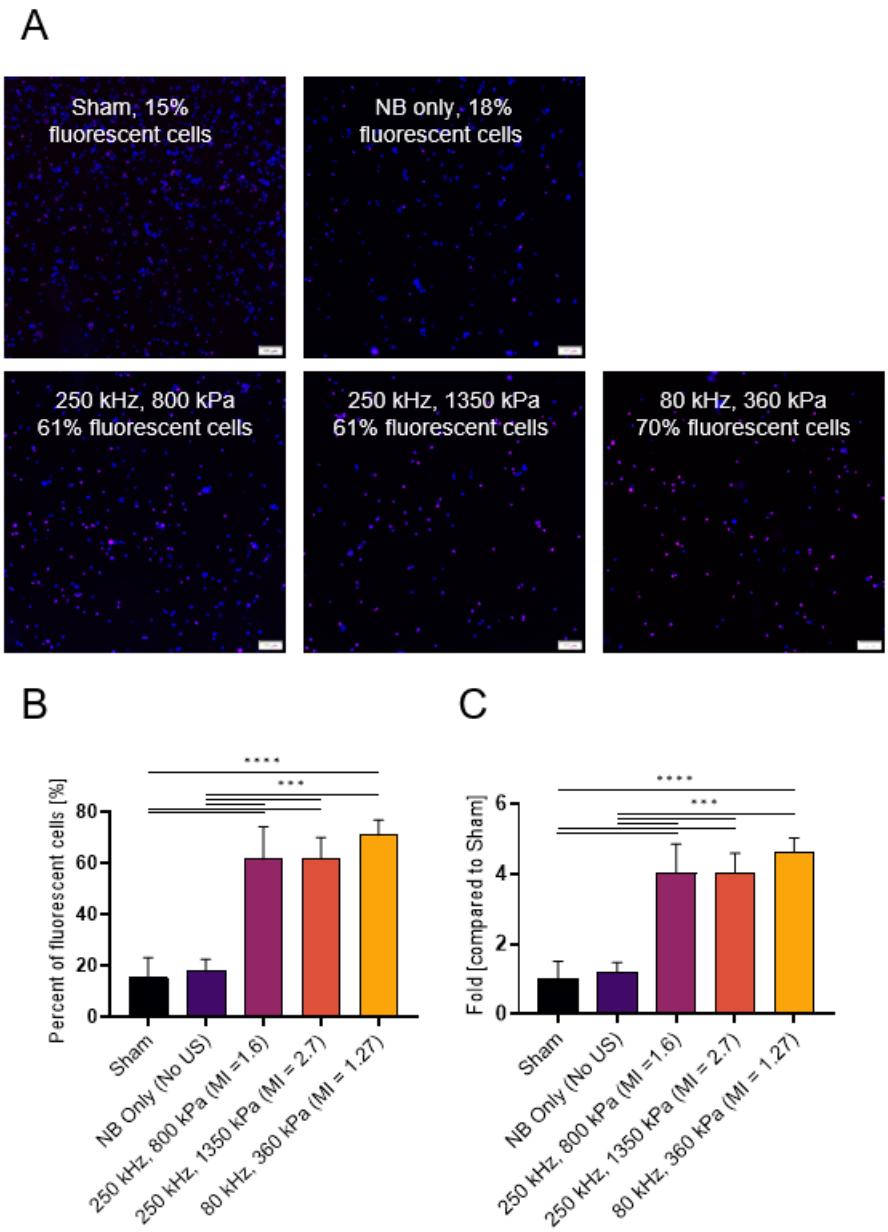

Figure 14 - NB sonoporation with 7-AAD. (A) Fluorescence microscopy overlay images for different ultrasound treatment groups. Scale bar is common to all subfigures in (A) and is 100 µm. (B) 7-AAD stained cells expressed as the percentage of live cells for the different groups. (C) The graph in (B) presented as fold uptake compared to the sham group. (B and C) One-way ANOVA with Tukey's multiple comparison test. Adjusted p values were *p<0.05, **p<0.01, ***p <0.001, ****p <0.0001. All data are plotted as the mean ± SD.

5.2.5.2 NB-mediated and MB-mediated sonoporation with FITC 4 kDa

The next molecule to be tested with NB was FITC-dextran 4 kDa. For this molecule size a center frequency of 250 kHz was used and pressures between 200 kPa and 800 kPa to correlate with the TMB sonoporation experiment. A group with free MB was also included in this experiment to compare between the free NB and free MB, and also to compare with the TMB sonoporation experiments.

NB only, without US treatment, did not show an increase in uptake compared to sham. A small non-significant increase in uptake started at 200 kPa (~10%), and then the significant increase was witnessed at 300 kPa. The same uptake was seen at 300, 500 and 800 kPa (~26%). Treatment with free MB and 500 kPa insonation did not affect the uptake. Results are presented in Fig. 15.

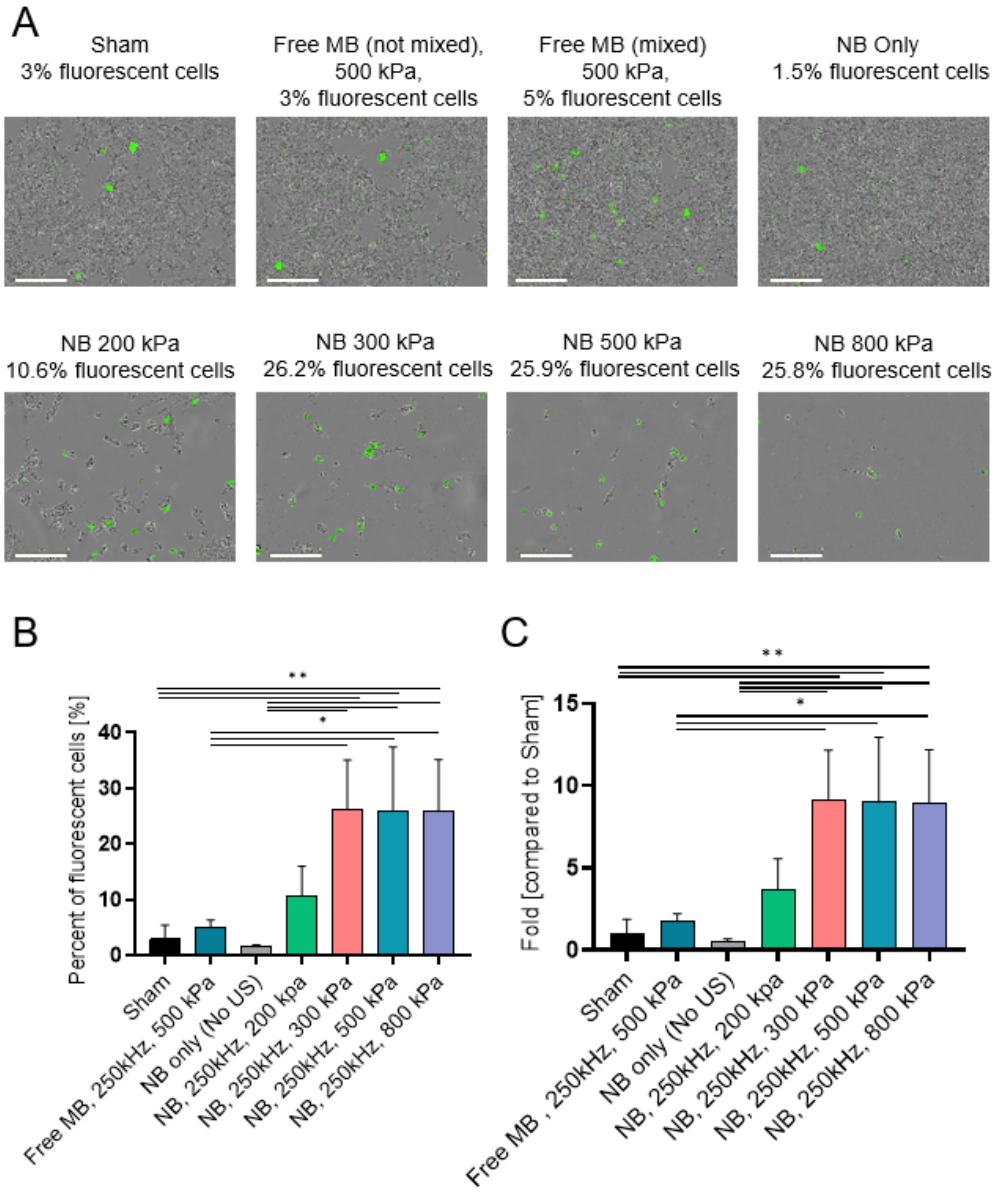

Figure 15 - Free MB and NB sonoporation with FITC 4 kDa. (A) Overlay images of cells and FITC 4 kDa for different ultrasound treatment groups. Each image presents a different PNP 1 day after sonoporation. Images were acquired by the Incucyte system with 20X magnification. Scale bar is common to all subfigures in (A) and is 200 µm. (B) FITC 4 kDa stained cells expressed as the percentage of live cells for the different treatment and control groups. (C) The graph in (B) presented as fold uptake compared to the sham group. (B and C) One-way ANOVA with Tukey's multiple comparison test.

5.2.5.3 NB, TMB and free MB sonoporation comparison

For a center frequency of 250 kHz and FITC-dextran 4 kDa a comparison of uptake percentage between free NB, free MB and TMB was done. When comparing between the NB and TMB for each PNP no significant change was witnessed, meaning by using free NB we can reach the same uptake as received with TMB.

A significant difference was witnessed between the groups with free MB and 500 kPa PNP, for which uptake was significantly low compared to the groups with free NB and groups with TMB at 500 kPa. This shows that TMB have a clear advantage over free MB when used for sonoporation, and also that free NB have an advantage over free MB. Results presented in Fig. 16.

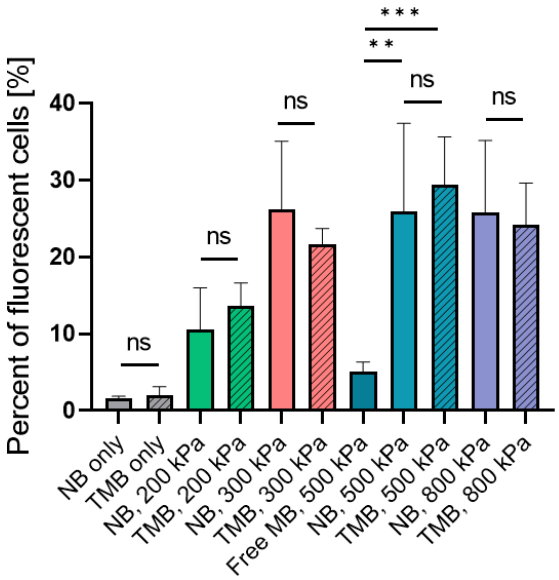

Figure 16 - Uptake comparison between TMB, free MB and NB. FITC 4 kDa stained cells expressed as the percentage of live cells for the different treatment and control groups. One-way ANOVA with Tukey's multiple comparison test. Adjusted p values were *p<0.05, **p<0.01, ***p <0.001, ****p <0.0001. All data are plotted as the mean ± SD.

5.3 Viability results

5.3.1 TMB viability results

Cell viability was evaluated for the treatment groups at multiple time points following sonoporation. For the 7-AAD molecule, cell viability was assessed immediately after sonoporation and demonstrated a similar viability of ~40% live cells for the different treatment groups. The Only US group had the same results as the sham group (Fig. 17A).

Unlike the 7-AAD, where the molecule uptake was assessed immediately after sonoporation, the FITC molecule uptake was evaluated 24 hrs. post sonoporation, Therefore, cell viability was assessed 24 hrs. post- sonoporation as well. For treatment with FITC 4 kDa, no significant difference was observed between the sham (100 ± 9.04%) and Only US (93.19 ± 11.9%) groups. In the treatment groups, viability dropped to 22.87 ± 1.01% for treatment only with TMB (no US application). Application of US + TMB further reduced viability from 22.57 ± 3.9% at a PNP of 100 kPa to 12.1 ± 0.92% and 7.92 ± 0.42% for treatment with 500 and 800 kPa, respectively (Fig. 17B). Cell recovery was assessed by evaluating cell viability 72 hrs. post sonoporation. Viability was significantly increased at 72 hrs. compared to 24 hrs. for all treated groups, reaching 52.84 ± 10.5% for the 500 kPa treatment. The sham and Only US groups remained similar, as did the Only TMB group (85.83 ± 2.17%) and the TMB with 100 kPa US (85.73 ± 1.67%). (Fig. 17C).

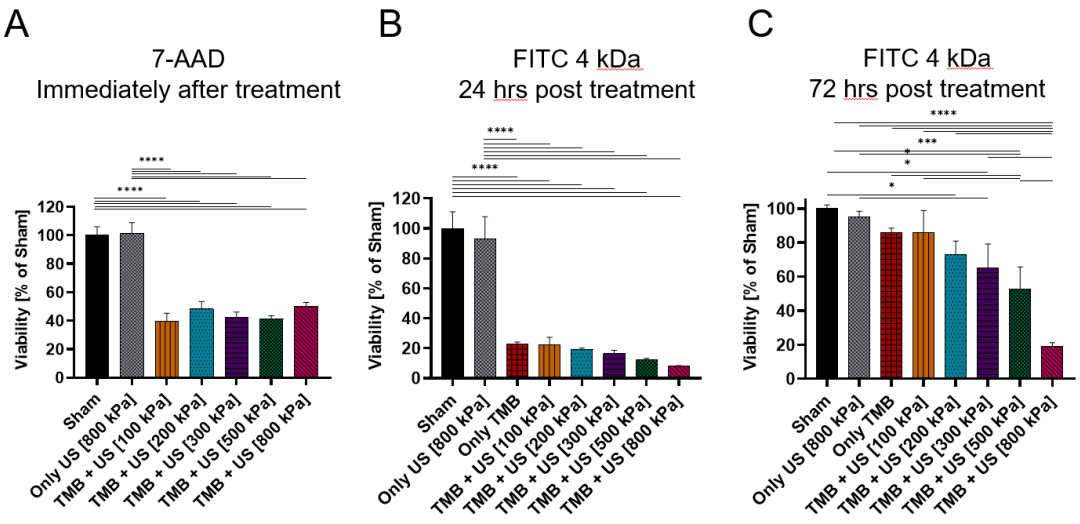

Figure 17 - Cell viability post treatment with TMB. (A) Viability of cells expressed as the percentage of the sham group for the different treatment and control groups immediately after sonoporation with 7-AAD. (B) Viability of cells expressed as the percentage of sham group for the different treatment and control groups 1 day after sonoporation with FITC 4 kDa. (C) Viability of cells expressed as the percentage of sham group for the different treatment and control groups 3 days after sonoporation with FITC 4 kDa. One-way ANOVA with Tukey's multiple comparison test. Adjusted p values were *p<0.05, **p<0.01, ***p <0.001, ****p <0.0001. All data are plotted as the mean ± SD.

5.3.2 Free NB and free MB viability results

Cells viability for sonoporation experiment with FITC 4 kDa at a center frequency of 250 kHz was also evaluated 24 hours post treatment with free MB and free NB. For treatment with NB only, no US application, viability remained the same as the sham group. For treatment with free MB at 500 kPa PNP viability was reduced to 82.24 ± 3.6%. However, the significant decrease in viability was witnessed for the NB treatment groups. Viability of 42.33 ± 12.98% was seen for PNP of 200 kPa and viability of 8.95 ± 2.78%, 3.61 ± 1.48% and 2.57 ± 0.27% was received for 300, 500 and 800 kPa respectively (Fig. 18).

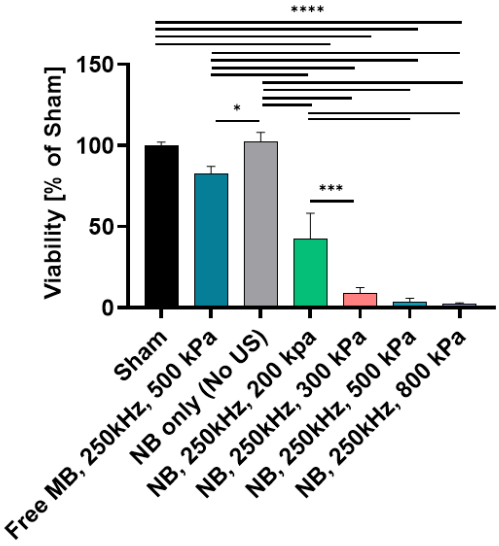

Figure 18 - Cell viability post treatment with NB. Viability of cells expressed as the percentage of sham group for the different treatment and control groups 1 day after sonoporation with FITC 4 kDa. One-way ANOVA with Tukey's multiple comparison test. Adjusted p values were *p<0.05, **p<0.01, ***p <0.001, ****p <0.0001. All data are plotted as the mean ± SD.

6 Discussion

Sonoporation is a growing field which has documented advantages over other delivery methods such as electroporation and viral vectors [69]. The clinical applications of sonoporation include drug and gene delivery for different cell types and locations [27], [43], [45], [9], [70]–[72]. To enhance this therapeutic platform, a better understanding of the relationship between the insonation parameters and the delivered material size is crucial. For example, sonoporation can be used to increase the spatiotemporal precision of the delivery of anti-cancer drugs. To do so, a large number of cancer cells need to be sonoporated to successfully impact the majority of the cancer cells, and a high delivery efficacy is required to maximize the drug concentration within the cells. Most optimization studies in this field have implemented frequencies exceeding 1 MHz; however, recent studies show the

advantages of using lower frequencies. The use of a center frequency of 250 kHz is particularly important, since these systems have entered clinical use. This low frequency advantages lie in the large focal spot that enables to treat a large volume of the tumor simultaneously, the increased penetration depth, its reduced attenuation and distortion, and improved beam steering capabilities. Notably, for brain therapy applications, the lower frequency aids in focusing through the human skull with minimal distortion and attenuation. Low frequency US was used to treat over 500 patients for brain indications applications. The high amplitude MB oscillations that occur at this low frequency can be used to develop mechanically-induced bioeffects at low PNPs, such as low energy bubble-mediated histotripsy [7], [12]. Here, it was shown that coupled with low frequency excitation, MBs can be used as mechanical therapeutic warheads that generate sufficiently large pores in cancer cell membranes to deliver large molecules. Most of the sonoporation studies are performed at megahertz frequencies where strong MB oscillations require PNP that exceed the FDA safety threshold. Most studies at higher frequencies have focused on the delivery of a single molecule with a constant diameter. Here we assessed the impact of molecular weight on delivery efficacy at a low frequency of 250 kHz, while using the same setup, to facilitate a direct comparison between molecules. Four molecules with molecular weights of 1.2, 4, 20 and 70 kDa were tested. These molecular weights are clinically important. The smaller molecular weights represent small anticancer drugs such as chemotherapy (<1 kDa) [41], [73]. 20 kDa molecules, for example, match siRNA and miRNA (~14 kDa) [71], [74]–[76], whereas 70 kDa corresponds to the size of proteins, macromolecules and genes [42]–[45]. Since the hydrodynamic radius of the molecule is not directly proportional to its molecular mass, the delivery of other types of molecules with similar molecular weight but with a different shape, might require further optimization. In the case of cancer therapy, alongside high delivery efficacy, the associated goal is to reduce cell viability, since

minimizing the tumor burden plays an important role in the success of cancer treatment [49]. The high MB expansion ratio caused by low frequency insonation makes it possible to reduce cell viability while creating large pores in cell membranes that facilitate drug delivery. Although this thesis dealt with the sonoporation of cancer cells, future applications could include the sonoporation of other cell types, such as immune cells, muscle cells and endothelial cells [71].

Numerical simulations were performed to estimate the required PNPs for MB with initial diameter of 1.5 μm. The results indicated that above a PNP of 200 kPa, inertial cavitation occurs, which is likely to increase cellular uptake as a result of pore formation via TMB collapse. The experimental results confirmed the theoretical predictions. For all molecule sizes, a large increase in the fraction of fluorescent cells was observed at a PNP of 200 kPa, compared to 100 kPa where the MBs were predicted to oscillate in stable cavitation. This clearly suggests that inertial cavitation plays a significant role in the successful sonoporation of cancer cells, unlike other cell types such as muscle cells where stable cavitation suffices [46].

The main focus here was on TMB-mediated sonoporation, for which fluorescent cells percentage was the highest for the smallest molecules, with ~58% of live cells for the 7-AAD molecule with a molecular weight of 1.2 kDa, at a PNP of 500 kPa. For the same PNP, the fraction of fluorescent cells was 29, 10 and 5% of live cells for FITC molecules with a molecular weight of 4, 20 and 70 kDa, respectively. However, when presenting the results as fold uptake compared to the sham group showed the reverse trend. For a PNP of 500 kPa, the largest molecule of 70 kDa yielded a 21.5-fold higher uptake compared to the sham group, whereas for the 1.2 kDa molecule, a 2.8-fold uptake was observed. This is due to the fact that the uptake in the sham groups decreased significantly as the molecular weight of the delivered molecule increased. The fraction of fluorescent cells was used here as the

metric to evaluate the delivery efficacy and compare between the different molecules' delivery. Alternatively, the number of molecules that were taken up by the cells can be quantified for drug delivery and therapeutic outcome assessment.

The experiments were conducted in Eppendorf tubes due the physical dimensions of the transducer's focal spot. For the center frequency of 250 kHz, the full width at half maximum for the lateral and axial axes were 7 x 50 mm, respectively. Taking advantage of the Eppendorf and focal elongated shapes, enables to conduct the treatment in these tubes, while treating the entire volume simultaneously without the need to mechanically move the transducer, as required in case of using adherent cells in plates. In vivo, the TMB can either be intravenously injected into the blood vessels, and interact with the endothelial cells, or can be locally injected directly into the tumor, and bind to cancer cells. The scenario that is mimicked in vitro resembles the intratumoral injection [7]. Under this condition, the entire tumor volume can be treated simultaneously using a single low frequency focused US application. The cell culturing is performed in plates, and following the US treatment, the cells are transferred back to 24-well plates. In addition, the same procedures that the treated groups undergo, are conducted also in the control groups.

The PNPs ranged from 0 to 800 kPa. The upper limit was chosen to remain below the FDA mechanical index limit of 1.9 [21], [77]. For all molecule sizes, at low PNPs, the fraction of fluorescent cells increased as a function of the PNP. However, beyond a PNP of 500 kPa, increasing the PNP to 800 kPa did not increase the fluorescent cells percentage significantly. This suggests that 500 kPa is the optimal PNP for sonoporation at a center frequency of 250 kHz. The expected expansion ratio for a PNP of 500 kPa is 33, and for 800 kPa is 50. These high expansions are both likely to create large pores in the cell membrane, thus increasing the PNP to 800 kPa, which does not affect delivery efficacy, but reduces cell viability .

Viability experiments were performed at three time points that match the fluorescence experiments time points, due to technical differences between the dyes and procedures. The smallest molecule (7-AAD, 1.2 kDa) is a fluorescent dye that undergoes a spectral shift upon association with DNA. Therefore, following sonoporation, the fluorescent signal arises only from the stained cells and does not exist in the background suspension. Consequently, fluorescence microscopy can be used immediately after the treatment to visualize and quantify the percentage of fluorescent cells. Unlike 7-AAD, FITC-dextran fluoresces on its own, and high background signal existed in the background suspension immediately after treatment. In order to remove background suspension, after the US treatment, the cells suspension was cultured for additional 24 hrs in plates. During this time, the cells adhered to the plate, and the media was washed and replaced to remove all fluorescent background signal. Therefore, 4, 20 and 70 kDa FITC-dextrans fluorescence and viability tests were performed 24 hours post treatment. An additional viability test was performed 72 hours post treatment to evaluate cells recovery as a function of time.

Immediately after treatment, cell viability was ~40% for all of the treatment groups. However, it dropped to below 20% after 24 hours. This suggests that cell death post-sonoporation requires time. Importantly, cells recovered their viability 72 hours post-treatment, where viability increased to 52% for the group treated with 500 kPa US and TMB. For cancer cell sonoporation, low viability is an advantage to reduce tumor burden. Therefore, a similar optimization needs to be achieved for sonoporation of other types of cells .

To achieve localization of the sonoporation effect targeting methods can be employed. When using MBs, a biotin-avidin link with antibody was used to attach the MBs to the cell surface, creating TMBs. The results showed that by using this targeting approach the sonoporation effect was significantly enhanced, resulting in ~29% uptake for treatment with FITC 4 kDa,

TMBs and 500 kPa PNP, while for the same treatment with free MBs an uptake of only ~5% was witnessed.

After TMB-sonoporation method was established and results were reviewed, it was decided to investigate how the low frequency US will affect NB-mediated sonoporation. This approach was based on the advantages that free NBs have over free MBs and targeted MBs. NBs are advantageous over MBs since there is no fear of the NBs blocking the small vasculature and they are known to accumulate at the tumor site as a result of the EPR effect [50],[51]. Therefore, systemic administration of NBs is sufficient for them to reach the tumor in almost every location inside the body, which cannot be achieved with MBs. Due to the size of MBs they need to be injected directly to the tumor location to achieve the necessary proximity between the MBs and the tumor cells to achieve the sonoporation effect. Also, NBs do not immediately float away from the cells as MBs do, therefore free NBs can be used with no additional targeting preparation steps as for targeted MBs.

NB-mediated sonoporation showed a similar uptake as the TMBs, with ~26% uptake of FITC 4 kDa at 500 kPa PNP. In addition, it was also shown that for treatment with free NBs, an uptake of ~26% was already reached even at a pressure of 300 kPa at 250 kHz. This means that with free NB, that can better accumulate at the tumor specific location, we can even use MI of 0.6, which is lower that the optimal MI for TMBs (uptake of ~29%) which was received for 250 kHz and 500 kPa, meaning MI = 1.

In vitro studies are considered a prerequisite prior to in vivo studies. The optimization results obtained here will be used in future in vivo studies, to assess delivery efficacy in a tumor model in mice. In vivo, additional factors could affect sonoporation efficacy such as the surrounding media's viscoelasticity [10], cell shape and connections [39] and also individual patients' variations in age, body mass index and many other factors. However, previous studies with 250 kHz US insonation have shown good agreement between in vitro and in

vivo results [27], [7]. This model can be used to not only identify the relationship between the delivered molecule size and the insonation parameters, but also to adjust the sonoporation parameters to different tumors in different subjects. In addition, with the vast number of multidrug treatments that are increasingly used, this platform can facilitate the comparison between different molecules delivery ranging from smaller chemotherapeutic drugs but also for larger complex drug carriers.

7 Conclusion and future work

This study optimized low frequency sonoporation efficacy by identifying the relationship between the delivered molecule size and the insonation parameters using the same acoustical setup. The development of low frequency MB or NB mediated ultrasound can be used as a highly effective drug delivery platform of large molecules with high spatiotemporal precision. The results confirmed that the optimal PNP for molecule delivery with TMBs at a center frequency of 250 kHz is 500 kPa. For FITC 4 kDa delivery with NBs at a center frequency of 250 kHz the highest fraction of fluorescent cells was already witnessed at 300 kPa. In general, the highest uptake was obtained for the smallest molecule, and dropped as the molecule size increased. However, since the baseline in the sham group was the lowest, delivery uptake presented in folds compared to sham was the highest for the largest molecule.

Future in-vivo studies can use the results attained here to optimize delivery to tumor model in mice. The results obtained for sonoporation with free NBs can promote the research while using lower MI and relying on the EPR effect without the need to target the MBs specifically to the tumor cells.

Overall, the use of low frequency and low MI enables the efficient delivery of different sized molecules, while reducing cancer cell viability. This approach can be used in the future as a combined method to maximize the therapeutic effects of cancer treatment.

8 References

[1] T. L. Szabo, *Diagnostic Ultrasound Imaging: Inside Out, 2nd ed.* 2013.

[2] L. G. Leal, "Bubble dynamics in time-periodic straining flows," *J. Fluid Mech.*, vol. 218, pp. 41–69, 1990, doi: 10.1017/S0022112090000921.

[3] E. A. Neppiras and B. E. Noltingk, "Cavitation produced by ultrasonics: Theoretical conditions for the onset of cavitation," *Proc. Phys. Soc. Sect. B*, vol. 64, no. 12, pp. 1032–1038, 1951, doi: 10.1088/0370-1301/64/12/302.

[4] S. Qin and K. W. Ferrara, "The Natural Frequency of Nonlinear Oscillation of Ultrasound Contrast Agents in Microvessels," *Ultrasound Med. Biol.*, vol. 33, no. 7, pp. 1140–1148, 2007, doi: 10.1016/j.ultrasmedbio.2006.12.009.

[5] M. FAN, D. TAO, R. HONAKER, and Z. LUO, "Nanobubble generation and its application in froth flotation (part I): nanobubble generation and its effects on properties of microbubble and millimeter scale bubble solutions," *Min. Sci. Technol.*, vol. 20, no. 1, pp. 1–19, 2010, doi: 10.1016/S1674-5264(09)60154-X.

[6] D. L. Miller, N. B. Smith, M. R. Bailey, G. J. Czarnota, K. Hynynen, and I. R. S. Makin, "Overview of therapeutic ultrasound applications and safety considerations," *J. Ultrasound Med.*, vol. 31, no. 4, pp. 623–634, 2012, doi: 10.7863/jum.2012.31.4.623.

[7] M. Bismuth, S. Katz, H. Rosenblatt, M. Twito, R. Aronovich, and T. Ilovitsh, "Acoustically Detonated Microbubbles Coupled with Low Frequency Insonation: Multiparameter Evaluation of Low Energy Mechanical Ablation," *Bioconjug. Chem.*, vol. 33 (6), pp. 1069–1079, 2022, doi: 10.1021/acs.bioconjchem.1c00203.

[8] Z. X. Chong, S. K. Yeap, and W. Y. Ho, “Transfection types, methods and strategies: A technical review,” *PeerJ*, vol. 9, pp. 1–37, 2021, doi: 10.7717/peerj.11165.

[9] J. Sitta and C. M. Howard, “Applications of ultrasound-mediated drug delivery and gene therapy,” *Int. J. Mol. Sci.*, vol. 22, no. 21, 2021, doi: 10.3390/ijms222111491.

[10] Y. Yang, Q. Li, X. Guo, J. Tu, and D. Zhang, “Mechanisms underlying sonoporation: Interaction between microbubbles and cells,” *Ultrason. Sonochem.*, vol. 67, p. 105096, 2020.

[11] P. Qin, T. Han, A. C. H. Yu, and L. Xu, “Mechanistic understanding the bioe ff ects of ultrasound-driven microbubbles to enhance macromolecule delivery,” *J. Control. Release*, vol. 272, no. January, pp. 169–181, 2018, doi: 10.1016/j.jconrel.2018.01.001.

[12] M. Bismuth *et al.*, “Low frequency nanobubble-enhanced ultrasound mechanotherapy for noninvasive cancer surgery,” *Nanoscale*, vol. 14, pp. 13614–13627, 2022, doi: 10.1039/D2NR01367C.

[13] P. Wawryka, A. Kiełbik, and G. Iwanek, “Microbubble based sonoporation — from the basics into clinical implications,” *Med. Res. J.*, vol. Volume 4, pp. 178–183, 2019.

[14] T. Ilovitsh *et al.*, “Enhanced microbubble contrast agent oscillation following 250 kHz insonation,” *Sci. Rep.*, vol. 8, no. 1, pp. 1–15, 2018, doi: 10.1038/s41598-018-34494-5.

[15] Z. Fan, R. E. Kumon, and C. X. Deng, “Mechanisms of microbubble-facilitated

sonoporation for drug and gene delivery," *Ther. Deliv.*, vol. 5, no. 4, pp. 467–486, 2014, doi: 10.4155/tde.14.10.

[16] P. Marmottant *et al.*, "A model for large amplitude oscillations of coated bubbles accounting for buckling and rupture," *J. Acoust. Soc. Am.*, vol. 118, no. 6, pp. 3499–3505, 2005, doi: 10.1121/1.2109427.

[17] S. A. G. Langeveld, B. Meijlink, A. F. W. Van Der Steen, N. De Jong, M. D. Verweij, and K. Kooiman, "Internalization of targeted microbubbles by endothelial cells and drug delivery by pores and tunnels," *J Control Release*, vol. 347, no. December 2021, pp. 460–475, 2022, doi: 10.1016/j.jconrel.2022.05.008.

[18] K. Ferrara, R. Pollard, and M. Borden, "Ultrasound microbubble contrast agents: Fundamentals and application to gene and drug delivery," *Annu. Rev. Biomed. Eng.*, vol. 9, pp. 415–447, 2007, doi: 10.1146/annurev.bioeng.8.061505.095852.

[19] A. Van Wamel *et al.*, "Vibrating microbubbles poking individual cells : Drug transfer into cells via sonoporation," *J. Control. Release*, vol. 112, no. 2, pp. 149–155, 2006, doi: 10.1016/j.jconrel.2006.02.007.

[20] E. Stride, "Physical principles of microbubbles for ultrasound imaging and therapy," *Cerebrovasc. Dis.*, vol. 27, no. SUPPL. 2, pp. 1–13, 2009, doi: 10.1159/000203122.

[21] S. M. Chowdhury, L. Abou-elkacem, T. Lee, J. Dahl, and A. M. Lutz, "Ultrasound and microbubble mediated therapeutic delivery : Underlying mechanisms and future outlook," *J. Control. Release*, vol. 326, no. June, pp. 75–90, 2020, doi: 10.1016/j.jconrel.2020.06.008.

[22] R. Karshafian, *On the Permeabilisation and Disruption of Cell Membranes by*

Ultrasound and Microbubbles, University of Toronto, 2010.

[23] M. Duvshani-Eshet and M. Machluf, “Therapeutic ultrasound optimization for gene delivery: A key factor achieving nuclear DNA localization,” *J. Control. Release*, vol. 108, no. 2–3, pp. 513–528, 2005, doi: 10.1016/j.jconrel.2005.08.025.

[24] Y. S. Li, E. Davidson, C. N. Reid, and A. P. McHale, “Optimising ultrasound-mediated gene transfer (sonoporation) in vitro and prolonged expression of a transgene in vivo: Potential applications for gene therapy of cancer,” *Cancer Lett.*, vol. 273, no. 1, pp. 62–69, 2009, doi: 10.1016/j.canlet.2008.07.030.

[25] B. D. M. Meijering, R. H. Henning, W. H. Van Gilst, I. Gavrilovic, A. Van Wamel, and L. E. Deelman, “Optimization of ultrasound and microbubbles targeted gene delivery to cultured primary endothelial cells,” *J. Drug Target.*, vol. 15, no. 10, pp. 664–671, 2007, doi: 10.1080/10611860701605088.

[26] A. V. Telichko *et al.*, “Therapeutic Ultrasound Parameter Optimization for Drug Delivery Applied to a Murine Model of Hepatocellular Carcinoma,” *Ultrasound Med. Biol.*, vol. 47, no. 2, pp. 309–322, 2021, doi: 10.1016/j.ultrasmedbio.2020.09.009.

[27] T. Ilovitsh *et al.*, “Low-frequency ultrasound-mediated cytokine transfection enhances T cell recruitment at local and distant tumor sites,” *Proc. Natl. Acad. Sci. U. S. A.*, vol. 117, no. 23, pp. 12674–12685, 2020, doi: 10.1073/pnas.1914906117.

[28] A. Harkin, A. Nadim, and T. J. Kaper, “On acoustic cavitation of slightly subcritical bubbles,” *Phys. Fluids*, vol. 11, no. 2, pp. 274–287, 1999, doi: 10.1063/1.869878.

[29] F. G. Blake, “The onset of cavitation in liquids: I,” Harvard University, 1949. Tech.

Memo, 1949.

[30] W. Lauterborn, “Numerical investigation of nonlinear oscillations of gas bubbles in liquids,” *J. Acoust. Soc. Am.*, vol. 59, no. 2, pp. 283–293, 1976, doi: 10.1121/1.380884.

[31] B. Glickstein, M. Levron, S. Shitrit, R. Aronovich, Y. Feng, and T. Ilovitsh, “Nanodroplet-Mediated Low-Energy Mechanical Ultrasound Surgery,” *Ultrasound Med. Biol.*, vol. 48, no. 7, pp. 1229–1239, 2022, doi: 10.1016/j.ultrasmedbio.2022.02.018.

[32] W. K. Bai, W. Zhang, B. Hu, and T. Ying, “Liposome-mediated transfection of wild-type P53 DNA into human prostate cancer cells is improved by low-frequency ultrasound combined with microbubbles,” *Oncol. Lett.*, vol. 11, no. 6, pp. 3829–3834, 2016, doi: 10.3892/ol.2016.4477.

[33] W. Zhang, S. liang Nan, W. kun Bai, and B. Hu, “Low-frequency ultrasound combined with microbubbles improves gene transfection in prostate cancer cells in vitro and in vivo,” *Asia. Pac. J. Clin. Oncol.*, no. September 2020, pp. 1–6, 2021, doi: 10.1111/ajco.13521.

[34] Z. Fan, H. Liu, M. Mayer, and C. X. Deng, “Spatiotemporally controlled single cell sonoporation,” *Proc. Natl. Acad. Sci. U. S. A.*, vol. 109, no. 41, pp. 16486–16491, 2012, doi: 10.1073/pnas.1208198109.

[35] L. Meng *et al.*, “Sonoporation of Cells by a Parallel Stable Cavitation Microbubble Array,” *Adv. Sci.*, vol. 6, no. 17, 2019, doi: 10.1002/advs.201900557.

[36] M. Wang, Y. Zhang, C. Cai, J. Tu, X. Guo, and D. Zhang, “Sonoporation-induced

cell membrane permeabilization and cytoskeleton disassembly at varied acoustic and microbubble-cell parameters," *Sci. Rep.*, vol. 8, no. 1, pp. 1–13, 2018, doi: 10.1038/s41598-018-22056-8.

[37] I. Beekers *et al.*, "Opening of endothelial cell–cell contacts due to sonoporation," *J. Control. Release*, vol. 322, no. January, pp. 426–438, 2020, doi: 10.1016/j.jconrel.2020.03.038.

[38] B. Helfield, X. Chen, S. C. Watkins, and F. S. Villanueva, "Biophysical insight into mechanisms of sonoporation," *Proc. Natl. Acad. Sci. U. S. A.*, vol. 113, no. 36, pp. 9983–9988, 2016, doi: 10.1073/pnas.1606915113.

[39] J. Park, Z. Fan, and C. X. Deng, "Effects of shear stress cultivation on cell membrane disruption and intracellular calcium concentration in sonoporation of endothelial cells," *J. Biomech.*, vol. 44, no. 1, pp. 164–169, 2011, doi: 10.1016/j.jbiomech.2010.09.003.

[40] I. Skachkov, Y. Luan, A. F. W. Van Der Steen, N. De Jong, and K. Kooiman, "Targeted microbubble mediated sonoporation of endothelial cells in vivo," *IEEE Trans. Ultrason. Ferroelectr. Freq. Control*, vol. 61, no. 10, pp. 1661–1667, 2014, doi: 10.1109/TUFFC.2014.006440.

[41] M. Maciulevičius, M. Tamošiūnas, D. Navickaitė, S. Šatkauskas, and M. S. Venslauskas, "Free- and Liposomal- Doxorubicin Delivery Via Microbubble Inertial Cavitation," *J. Drug Deliv. Sci. Technol.*, vol. 72, no. May, 2022, doi: 10.2139/ssrn.3981539.

[42] X. Liu, F. Wu, Y. Ji, and L. Yin, "Recent Advances in Anti-cancer Protein/Peptide Delivery," *Bioconjug. Chem.*, vol. 30, no. 2, pp. 305–324, 2019, doi:

10.1021/acs.bioconjchem.8b00750.

[43] M. R. Dreher, W. Liu, C. R. Michelich, M. W. Dewhirst, F. Yuan, and A. Chilkoti, "Tumor vascular permeability, accumulation, and penetration of macromolecular drug carriers," *J. Natl. Cancer Inst.*, vol. 98, no. 5, pp. 335–344, 2006, doi: 10.1093/jnci/djj070.

[44] W. Matsunaga, M. Ichikawa, A. Nakamura, T. Ishikawa, and A. Gotoh, "Lentiviral vector-mediated gene transfer in human bladder cancer cell lines," *Anticancer Res.*, vol. 38, no. 4, pp. 2015–2020, 2018, doi: 10.21873/anticanres.12440.

[45] Y. Wang *et al.*, "Upregulation of ULK1 expression in PC-3 cells following tumor protein P53 transfection by sonoporation," *Oncol. Lett.*, vol. 11, no. 1, pp. 699–704, 2016, doi: 10.3892/ol.2015.3946.

[46] K.-C. Tsai *et al.*, "Differences in gene expression between sonoporation in tumor and in muscle," *J. Gene Med.*, vol. 14, no. 1, pp. 44–53, 2012, doi: 10.1002/jgm.

[47] Y. Tian *et al.*, "New aspects of ultrasound-mediated targeted delivery and therapy for cancer," *Int. J. Nanomedicine*, vol. 15, pp. 401–418, 2020, doi: 10.2147/IJN.S201208.

[48] A. Delalande, S. Kotopoulis, M. Postema, P. Midoux, and C. Pichon, "Sonoporation: Mechanistic insights and ongoing challenges for gene transfer," *Gene*, vol. 525, no. 2, pp. 191–199, 2013, doi: 10.1016/j.gene.2013.03.095.

[49] A. C. Huang *et al.*, "T-cell invigoration to tumour burden ratio associated with anti-PD-1 response," *Nature*, vol. 545, no. 7652, pp. 60–65, 2017, doi: 10.1038/nature22079.

[50] R. Abdalkader *et al.*, “The development of mechanically formed stable nanobubbles intended for sonoporation-mediated gene transfection The development of mechanically formed stable nanobubbles intended for sonoporation-mediated gene transfection,” *Drug Deliv.*, vol. 24, no. 1, pp. 320–327, 2017, doi: 10.1080/10717544.2016.1250139.

[51] A. Prabhakar and R. Banerjee, “Nanobubble Liposome Complexes for Diagnostic Imaging and Ultrasound-Triggered Drug Delivery in Cancers : A Theranostic Approach,” *ACS Omega*, vol. 4, no. 13, pp. 15567–15580, 2019, doi: 10.1021/acsomega.9b01924.

[52] J. Park, Y. Choi, H. Chang, W. Um, J. H. Ryu, and I. Chan, “Theranostics Alliance with EPR Effect : Combined Strategies to Improve the EPR Effect in the Tumor Microenvironment,” *Theranostics*, vol. 9, no. 26, pp. 8073–8090, 2019, doi: 10.7150/thno.37198.

[53] J. Vanosdol *et al.*, “Sequential HIFU heating and nanobubble encapsulation provide ef fi cient drug penetration from stealth and temperature sensitive liposomes in colon cancer,” *J. Control. Release*, vol. 247, pp. 55–63, 2017, doi: 10.1016/j.jconrel.2016.12.033.

[54] K. Nishimura, S. Fumoto, Y. Fuchigami, M. Hagimori, K. Maruyama, and S. Kawakami, “Effective intraperitoneal gene transfection system using nanobubbles and ultrasound irradiation,” *Drug Deliv.*, vol. 24, no. 1, pp. 737–744, 2017, doi: 10.1080/10717544.2017.1319433.

[55] H. Kida *et al.*, “Nanobubble Mediated Gene Delivery in Conjunction With a Hand-Held Ultrasound Scanner,” *Front. Pharmacol.*, vol. 11, no. April, pp. 1–10, 2020,

doi: 10.3389/fphar.2020.00363.

[56] B. Zhang, M. Chen, Y. Zhang, W. Chen, L. Zhang, and L. Chen, “An ultrasonic nanobubble-mediated PNP/ fludarabine suicide gene system: A new approach for the treatment of hepatocellular carcinoma,” *PLoS One*, vol. 13, no. 5, pp. 1–15, 2018, doi: 10.1371/journal.pone.0196686.

[57] K. Nishimura *et al.*, “Application of direct sonoporation from a defined surface area of the peritoneum: Evaluation of transfection characteristics in mice,” *Pharmaceutics*, vol. 11, no. 5, 2019, doi: 10.3390/pharmaceutics11050244.

[58] B. Wu *et al.*, “Targeted nanobubbles in low-frequency ultrasound-mediated gene transfection and growth inhibition of hepatocellular carcinoma cells,” *Tumor Biol.*, vol. 37, no. 9, pp. 12113–12121, 2016, doi: 10.1007/s13277-016-5082-2.

[59] C. Hu, D. Jiang, M. Wu, J. Wang, and R. Zhang, “Ultrasound-mediated nanobubble destruction (UMND) facilitates the delivery of VEGFR2-targeted CD-TK-loaded cationic nanobubbles in the treatment of bladder cancer,” *J. Cancer Res. Clin. Oncol.*, vol. 146, no. 6, pp. 1415–1426, 2020, doi: 10.1007/s00432-020-03160-7.

[60] A. J. Sojahrood, R. Karshafian, and M. C. Kolios, “Detection and characterization of higher order nonlinearities in the oscillations of Definity at higher frequencies and very low acoustic pressures,” in *2012 IEEE International Ultrasonics Symposium*, 2012, pp. 1193–1196.

[61] C. Huang and J. T. Mason, “Geometric packing constraints in egg phosphatidylcholine vesicles,” *Proc. Natl. Acad. Sci. U. S. A.*, vol. 75, no. 1, pp. 308–310, 1978, doi: 10.1073/pnas.75.1.308.

[62] N. Kučerka, M. A. Kiselev, and P. Balgavý, “Determination of bilayer thickness and lipid surface area in unilamellar dimyristoylphosphatidylcholine vesicles from small-angle neutron scattering curves: A comparison of evaluation methods,” *Eur. Biophys. J.*, vol. 33, no. 4, pp. 328–334, 2004, doi: 10.1007/s00249-003-0349-0.

[63] G. Shi *et al.*, “Isolation of Rare Tumor Cells from Blood Cells with Buoyant Immuno-Microbubbles,” *PLoS One*, vol. 8, no. 3, 2013, doi: 10.1371/journal.pone.0058017.

[64] N. C. L. Zembruski, V. Stache, W. E. Haefeli, and J. Weiss, “7-Aminoactinomycin D for apoptosis staining in flow cytometry,” *Anal. Biochem.*, vol. 429, no. 1, pp. 79–81, 2012, doi: 10.1016/j.ab.2012.07.005.

[65] D. L. Miller, S. Bao, and J. E. Morris, “Sonoporation of cultured cells in the rotating tube exposure system,” *Ultrasound Med. Biol.*, vol. 25, no. 1, pp. 143–149, 1999, doi: 10.1016/S0301-5629(98)00137-9.

[66] R. Karshafian, S. Samac, P. D. Bevan, and P. N. Burns, “Microbubble mediated sonoporation of cells in suspension: Clonogenic viability and influence of molecular size on uptake,” *Ultrasonics*, vol. 50, no. 7, pp. 691–697, 2010, doi: 10.1016/j.ultras.2010.01.009.

[67] R. Karshafian, P. D. Bevan, R. Williams, S. Samac, and P. N. Burns, “Sonoporation by Ultrasound-Activated Microbubble Contrast Agents: Effect of Acoustic Exposure Parameters on Cell Membrane Permeability and Cell Viability,” *Ultrasound Med. Biol.*, vol. 35, no. 5, pp. 847–860, 2009, doi: 10.1016/j.ultrasmedbio.2008.10.013.

[68] B. D. M. Meijering *et al.*, “Ultrasound and microbubble-targeted delivery of

macromolecules is regulated by induction of endocytosis and pore formation," *Circ. Res.*, vol. 104, no. 5, pp. 679–687, 2009, doi: 10.1161/CIRCRESAHA.108.183806.

[69] L. J. M. Juffermans *et al.*, "Local drug and gene delivery through microbubbles and ultasound: a save and efficient alternative for viral vectors?," *Prog Cardiovasc Dis*, vol. 44, no. 1, pp. 45–54, 2001, [Online]. Available: http://www.ncbi.nlm.nih.gov/entrez/query.fcgi?cmd=Retrieve&db=PubMed&dopt=Citation&list_uids=11533926

[70] C. R. Lin *et al.*, "Sonoporation-mediated gene transfer into adult rat dorsal root ganglion cells," *J. Biomed. Sci.*, vol. 17, no. 1, pp. 2–7, 2010, doi: 10.1186/1423-0127-17-44.

[71] A. Karki *et al.*, "Sonoporation as an Approach for siRNA delivery into T cells," *Ultrasound Med. Biol.*, vol. 45, no. 12, pp. 3222–3231, 2019, doi: 10.1016/j.ultrasmedbio.2019.06.406.

[72] J. Xu, A. Singh, and M. M. Amiji, "Redox-responsive targeted gelatin nanoparticles for delivery of combination wt-p53 expressing plasmid DNA and gemcitabine in the treatment of pancreatic cancer," *BMC Cancer*, vol. 14, no. 1, pp. 1–12, 2014, doi: 10.1186/1471-2407-14-75.

[73] J. K. Jackson, F. N. Pirmoradi, C. P. L. Wan, T. Siu, M. Chiao, and H. M. Burt, "Increased accumulation of paclitaxel and doxorubicin in proliferating capillary cells and prostate cancer cells following ultrasound exposure," *Ultrasonics*, vol. 51, no. 8, pp. 932–939, 2011, doi: 10.1016/j.ultras.2011.05.008.

[74] C. H. Ha, S. C. Lee, S. Kim, J. Chung, H. Bae, and K. Kwon, "Novel mechanism of gene transfection by low-energy shock wave," *Sci. Rep.*, vol. 5, pp. 1–13, 2015, doi:

10.1038/srep12843.

[75] M. Kinoshita and K. Hynynen, “A novel method for the intracellular delivery of siRNA using microbubble-enhanced focused ultrasound,” *Biochem. Biophys. Res. Commun.*, vol. 335, no. 2, pp. 393–399, 2005, doi: 10.1016/j.bbrc.2005.07.101.

[76] S. Mullick Chowdhury *et al.*, “Ultrasound-guided therapeutic modulation of hepatocellular carcinoma using complementary microRNAs,” *J. Control. Release*, vol. 238, pp. 272–280, 2016, doi: 10.1016/j.jconrel.2016.08.005.

[77] K. B. Bader and C. K. Holland, “Gauging the likelihood of stable cavitation from ultrasound contrast agents,” *Phys. Med. Biol.*, vol. 58, no. 1, p. 127, 2012.

תקציר

באמצעות שילוב של גלי אולטרסאונד יחד עם בועיות גז ניתן לפעור חורים בממברנת התא וע"י כך לאפשר כניסת חומרים כגון תרופות וגנים, אשר אינם מסוגלים לחדור בד"כ. גורם משמעותי ביעילות העברת החומרים לתאים הוא גודלם ביחס לגודל החורים אשר נפערו בממברנת התא. העברה של מולקולות גדולות היא מאתגרת במיוחד ויכולה להשפיע על תוצאת הטיפול באופן משמעותי. על מנת לאפשר מעבר של מולקולות גדולות יחסית יש צורך לפעור חורים גדולים ביחס למולקולות קטנות יותר. אולטרסאונד סטנדרטי עושה שימוש בתדרים בתחום המגה-הרץ, אך לאחרונה מחקרים הראו ששהפעלת תדרים נמוכים של 250 קילו-הרץ על מיקרובועות (תדר בעל סדר גודל מתחת לתדר הרזוננס של המיקרובועיות), גורם להן לבצע תנודות עוצמתיות ומועצמות בהשוואה לתדרים בטווח המגה-הרץ. על מנת לשפר את יעילות ההעברה של מולקולות גדולות אנו מציעים שימוש בתדרים נמוכים ליצירת חורים גדולים בממברנת התא כתוצאה מתנודות הבועות גז באמפליטודה גבוהה בתדרים אלה. במחקר הנ"ל הערכנו את השפעת הסונופורציה בתדר נמוך בשילוב עם בועות גז מסוג מיקרו- וננו-בועות על חדירת מולקולות בגדלים שונים לתאי סרטן על-ידי אופטימיזציה של העברת ארבע מולקולות בגדלים הנעים בין 1.2 ל-70 קילודלתון. תהליך האופטימיזציה גילה כי לחץ האולטרסאונד האופטימלי היה 500 קילופסקל. העלאה נוספת של הלחץ לא שיפרה את אחוז כניסת החומרים לתאים ולמעשה רק הורידה את הויאביליות שלהם. עבור המולקולות הקטנות, בגודל 1.2 ו 4 קילו-דלתון, הקבוצות שטופלו בלחץ של 500 קילו-פסקל ומיקרובועיות הראו העברה של 58% ו- 29% בהתאמה, כאשר עבור המולקולות בגדלים 20 ו-70 קילו-דלתון נצפתה העברה של 10% ו- 5% בהתאמה. לאחר מכן פיתחנו שיטה משופרת שאינה דורשת שימוש בבועות אשר נקשרות לתאי הסרטן ע"י פיתוח ננובועות במקום מיקרובועות, ככלי לביצוע סונופורציה לא פולשנית. ע"י שימוש בשילוב של אולטרסאונד בתדר נמוך יחד עם ננובועות, הראנו כי עבור המולקולות בגודל 1.2 ו 4 קילו-דלתון, אנו מצליחים לקבל את אותו אחוז העברה כפי שהתקבל עם מיקרובועיות. השיטה הזו יכולה לאפשר התקדמות לניסויים במודל גידולים בעכברים בצורה לא פולשנית.הממצאים שלנו מראים שאולטרסאונד בתדר נמוך (250 קילוהרץ) גורם לתנודות באמפליטודה גבוהה in vitro, אשר משפרות את יעילות ההעברה של מולקולות גדולות. לסיכום ניתן לומר כי להעברה מוצלחת של מולקולות באמצעות אולטרסאונד נדרשת בחירה קפדנית של פרמטרי הטיפול על מנת למקסם את האפקט הטיפולי.

אוניברסיטת תל אביב

הפקולטה להנדסה ע"ש איבי ואלדר פליישמן

בית הספר לתארים מתקדמים ע"ש זנדמן-סליינר

סונופורציה באמצעות אולטרסאונד בתדר נמוך: מנגנון משופר לצורך העברת תרופות וגנים לתוך תאים

חיבור זה הוגש כעבודת גמר לקראת התואר "מוסמך אוניברסיטה" בהנדסה ביו-רפואית

על-ידי

מיכל אק

העבודה נעשתה במחלקה להנדסה ביו-רפואית

בהנחיית ד"ר טלי אילוביץ'

אוניברסיטת תל אביב

הפקולטה להנדסה ע"ש איבי ואלדר פליישמן

בית הספר לתארים מתקדמים ע"ש זנדמן-סליינר

סונופורציה באמצעות אולטרסאונד בתדר נמוך: מנגנון משופר לצורך העברת תרופות וגנים לתוך תאים

חיבור זה הוגש כעבודת גמר לקראת התואר "מוסמך אוניברסיטה" בהנדסה ביו-רפואית

על-ידי

מיכל אק

העבודה נעשתה במחלקה להנדסה ביו-רפואית

בהנחיית ד"ר טלי אילוביץ'